

Supporting Information Appendix for

Neuronal couplings between retinal ganglion cells inferred by efficient inverse statistical physics methods

S. Cocco, S. Leibler, R. Monasson

Table of contents:

1. Inference of couplings and of their accuracy within the inverse Ising model (page 2)
2. Limitations of the Ising model: higher-order correlations and couplings (page 7)
3. Algorithm for the Inverse Integrate-and-Fire Problem (page 11)
4. On Cross-correlograms: Analysis of Data, Relationship with Couplings, and Simulations (page 14)
5. Correspondence between Integrate-and-Fire and Ising Inverse Models (page 23)
6. Spatial features of the inferred couplings (page 28)
7. On states and the large- N limit in the inverse Ising model (page 36)
8. Bibliography and footnotes (page 39)

Supporting Information Appendix, Section 1:

Inference of couplings and of their accuracy within the inverse Ising model

I. INFERENCE AND MINIMIZATION OF THE ISING ENTROPY

A multi-electrode recording provides the firing times of N recorded cells during a time interval of duration T . In the Ising inverse approach the recording interval is divided into time windows (time-bins) of width Δt and the data are encoded in $T/\Delta t$ configurations $\mathbf{s} = (s_1, s_2, \dots, s_N)$ of the N binary variables s_i , ($i = 1, \dots, N$) called spins (by analogy with magnetic systems described by the Ising model). The value of each spin variable is: $s_i^\tau = 1$, if the cell i is active in the time-bin τ ($\tau = 1, \dots, B = T/\Delta t$), $s_i = 0$ otherwise. Let p_i be the probability that the cell i is active in a given time-bin, and p_{ij} be the joint probability that the cells i and j are both active in the same bin.

The Maximum Entropy Principle (MEP) states that the probabilistic model, $P(\mathbf{s})$, which reproduces the best the observed one cell $\{p_i\}$ and two-cell firing probabilities $\{p_{ij}\}$ in the time-bin, Δt , is the one that maximizes the entropy of the distribution

$$S[P] = - \sum_{\mathbf{s}} P(\mathbf{s}) \ln P(\mathbf{s}) \quad (1)$$

under the constraints that the average values of the spins and of the spin-spin correlations coincide with, respectively, the observed one-cell and two-cell firing probabilities [1, 13]. In practice, these constraints are enforced by introducing Lagrange multipliers:

$$S^{MEP}[\{p_i\}, \{p_{ij}\}] = \min_{h_i, J_{ij}, \lambda} \max_{P(\mathbf{s})} \left[S[P] + 2 \sum_i h_i \left(p_i - \sum_{\mathbf{s}} P(\mathbf{s}) s_i \right) + 4 \sum_{i < j} J_{ij} \left(p_{ij} - \sum_{\mathbf{s}} P(\mathbf{s}) s_i s_j \right) + \lambda \left(1 - \sum_{\mathbf{s}} P(\mathbf{s}) \right) \right]. \quad (2)$$

Note the presence of the additional multiplier λ to ensure the normalization of P . The maximization condition over $P[\mathbf{s}]$ shows that the MEP probability corresponds to the equilibrium Boltzmann-Gibbs distribution of the Ising model:

$$P(\mathbf{s}) = \frac{\exp(-E(\mathbf{s}))}{Z[\{h_i\}, \{J_{ij}\}]} \quad (3)$$

where E is the energy function of the Ising model

$$E(\mathbf{s}) = -4 \sum_{i < j} J_{ij} s_i s_j - 2 \sum_i h_i s_i \quad (4)$$

and

$$Z[\{h_i\}, \{J_{ij}\}] = \sum_{\mathbf{s}} \exp(-E(\mathbf{s})) \quad (5)$$

is its partition function. The optimal values for the Lagrange multipliers J_{ij} and h_i can therefore be interpreted in terms of the couplings and the fields of the Ising model. The presence of the factor 4 multiplying the couplings in eqs. (2) and (4) ensures that the couplings J_{ij} , defined here for the variables s_i taking values 0, 1, are equal to the couplings for the magnetic systems, in which spins take values ± 1 [1]. From eq. (2) the values of the couplings and fields are then found through the minimization [19] of

$$S[\{h_i\}, \{J_{ij}\}] = \log Z[\{h_i\}, \{J_{ij}\}] - 4 \sum_{i < j} J_{ij} p_{ij} - 2 \sum_i h_i p_i. \quad (6)$$

Since S is a convex function of its variables, the minimum is always well defined, however, it may be located at infinity. For a simple example of such a situation consider one spin ($N = 1$) with firing rate f . The probability p that

the spin variable equals 1 is then $p = 1 - \exp(-f\Delta t)$, and it is close to zero for time-bin widths Δt much smaller than the typical times between spikes, $1/f$. If the number B of time-bins is much smaller than $1/(f \times \Delta t)$ the spin is likely to be equal to 0 in all configurations. Hence, the measured firing probability is $p = 0$, and the field h , the solution of the inverse problem, would be $h = -\infty$. Similarly, if a pair of cells are never active together in the same time-bin (for all available configurations) the corresponding coupling will be infinite. This problem can be easily cured by adding to the Ising entropy an extra term:

$$S_M[\{h_i\}, \{J_{ij}\}] = S[\{h_i\}, \{J_{ij}\}] + \frac{\Gamma}{2} \left(\sum_{i<j} J_{ij}^2 + \sum_i h_i^2 \right). \quad (7)$$

While the Ising entropy S can be thought of as representing the cost of describing the data within the Ising model, the extra term in S_M is expressing the cost of describing the model itself: it is the length of the model in the language of Minimum Message Length (MML) theory [2]. This additional contribution has also a simple meaning in the Bayesian framework, where it represents minus the logarithm of the prior probability over the fields and couplings (chosen here to be Gaussian). The presence of a quadratic contribution in (7) ensures that S_M grows quickly to $+\infty$ when $N(N+1)/2$ fields and couplings get away from the origin. This proves the existence, uniqueness, and finiteness of the solution to our inverse problem. Note that the choice of the Gaussian prior is arbitrary; any log prior growing faster than linearly would be acceptable.

The parameter Γ in (7) is equal to $1/(B \sigma^2)$, where σ^2 is the variance of the *a priori* probability of the fields and couplings. For the data we find that the optimal value for Γ is of the order of 10^{-6} , *e.g.* for the Flicker stimulus (see below) $B = 2 \cdot 10^5$, and we have chosen $\sigma^2 = 5$. In practice, we observe that the choice of Γ does affect the values of a few couplings, but is irrelevant for most of the couplings and for all fields. The reason is intuitively clear from the discussion above: only the interactions between cells never spiking together, or with a very limited number of coinciding firing events will depend on Γ (see Figure 2 and the attached comments below). Note that Γ tends to zero for very large size B of the data set: the MEP couplings and fields always coincide with the MML predictions. Indeed, sampling is perfect in this limit.

II. AN INVERSE ALGORITHM TO OBTAIN THE VALUES OF COUPLINGS AND FIELDS

The calculation of the partition function Z , Eq. (5), requires, for a given set of fields and couplings, a computational effort growing exponentially with the number of cells. Therefore, the entropy S cannot be obtained directly using definition (6) for N exceeding, say, 15. Fortunately, since the time-bin width Δt (about 10 ms) is much smaller than the average spacing between spikes (more than 1 s for the analyzed recordings) the firing probabilities are close to zero, and we need to know S for large values of the fields h_i only. Therefore, we have extended the large-field expansions used in statistical physics of magnetic systems, so to:

1. deal with the case of non-uniform (cell-dependent) couplings and fields;
2. carry out the minimization over these (large) fields and the couplings in Eq. (7) in order to obtain S , and then S_M , at fixed one- and two-cell firing probabilities.

We briefly present the outcome of this large-field expansion, and how it can be turned into a practical algorithm to calculate the couplings J_{ij} and fields h_i as function of the firing probabilities p_i and the probability that two cells spikes in the same time window p_{ij} . For large fields, the entropy S can be hence decomposed into a sum of contributions coming from all the k -plets of distinct spins,

$$S[\{p_i\}, \{p_{ij}\}] = \sum_{k=1}^N \sum_{i_1 < i_2 < \dots < i_k} S_k[i_1, i_2, \dots, i_k; \{p_i\}, \{p_{ij}\}] \quad (8)$$

The first term S_1 in this expansion corresponds to the entropy of a single spin at fixed firing probability p_i ,

$$S_1[i; p_i] = -p_i \log p_i - (1 - p_i) \log(1 - p_i). \quad (9)$$

The second term, S_2 , represents the entropy of a system of two spins with imposed firing probabilities and pairwise firing probabilities minus the sum of the two single-spin contributions S_1 . Its exact expression is

$$\begin{aligned} S_2[i, j; p_i, p_j, p_{ij}] &= -p_{i,j} \log(p_{ij}) - (p_i - p_{i,j}) \log(p_i - p_{i,j}) \\ &\quad - (p_j - p_{i,j}) \log(p_j - p_{i,j}) - (1 - p_i - p_j + p_{i,j}) \log(1 - p_i - p_j + p_{i,j}). \end{aligned} \quad (10)$$

Higher- k terms have similar interpretations: informally speaking, S_k is the contribution to the entropy of a set of k spins (with their average values and correlations fixed, i.e. restricted by the corresponding k and $k(k-1)/2$ constraints)

that cannot be obtained from the entropies of smaller subsets of these k spins. Although for $k \geq 3$ we are not able to provide an analytical expression for S_k , we can calculate it numerically for small enough values of k . In practice, for $k \leq k_{max} = 7$, the sum over 2^k spin configurations in the partition function Z (5) can be explicitly evaluated, and the expression (6) can be minimized over the fields and couplings, leading to a high accuracy approximation for the entropy S .

For a given pair a, b of spins, we can consider all the subsets of $k = 2, 3, \dots, k_{max}$ spins containing this pair, $\mathcal{R}_k = (i_1, i_2, \dots, i_{k-2}, a, b)$, and for each such subset, we can calculate the value of the couplings $J_{ab}(\mathcal{R}_k)$ minimizing $S_k[\mathcal{R}_k; \{p_i\}, \{p_{ij}\}]$. The inferred coupling are then given by

$$J_{ab} = \sum_{k=2}^{k_{max}} (-1)^{k_{max}-k} \binom{N-k-1}{k_{max}-k} \sum_{\mathcal{R}_k} J_{ab}(\mathcal{R}_k). \quad (11)$$

The presence of the combinatorial factors with alternate signs in the above equation originates from the so-called exclusion-inclusion principle, which avoids multiple counting of the same contributions to the total coupling. A similar procedure provides us with the approximate values of the fields h_i .

The above expression is a good approximation for the true couplings as long as the contributions from the sets containing more than k_{max} spins are small. This is indeed the case for small time-bin widths Δt . To see this, let us assume that all firing probabilities p_i are small, i.e. $p_i < \epsilon$ for some $\epsilon > 0$; one may for instance chose $\epsilon = \max_i(f_i) \times \Delta t$, where f_i is the firing rate of cell i . Then $S_k < C_k \epsilon^k$, where C_k is a constant. As an example, it is easy to check from (10) that $S_2 = O(\epsilon^2)$. This property allows us to truncate the sum in (8) to the terms $k < k_{max}$ only, and to estimate the accuracy of the resulting approximation for the entropy, the couplings, and the fields.

III. TEST OF THE INVERSE ISING ALGORITHM

We have tested our inverse Ising algorithm on three published multi-electrode recordings from salamander ganglion cells:

- A recordings of the spontaneous activity of 60 cells observed during 2000 seconds in total darkness (here called Dark) [6].
- A 4450 second-long recording of 51 cells from the same retina illuminated with randomly flickering bright squares, hereafter called the Flicker stimulus [6]; 32 cells are common to Flicker and Dark data sets (both sets of data courtesy of M. Meister). The vast majority of these cells are of OFF-type.
- A recording from 40 cells in another retina presented with a 120 second-long natural movie repeated 20 times [1] (data courtesy of M. Berry).

Our test procedure was based on a comparison of the couplings and fields found with our inference algorithm and the ones obtained from an iterative numerical procedure, called Boltzmann learning in statistical inference literature [5]. The principle of this last procedure can be summarized as follows:

1. one starts from some presumed values for the fields h_i and couplings J_{ij} ;
2. based on these initial values and using a Monte Carlo routine, one calculates then the firing probabilities p_i and two-spin connected correlations $c_{ij} = p_{ij} - p_i p_j$;
3. one compares these values to their experimental counterparts, p_i^{exp} and c_{ij}^{exp} . The procedure is stopped if $|p_i - p_i^{exp}| < \epsilon$ for every cell i , and $|c_{ij} - c_{ij}^{exp}| < \epsilon$ for every pair i, j , where ϵ is the desired accuracy. Otherwise the fields and couplings are updated accordingly, e.g. J_{ij} is increased if $c_{ij} < c_{ij}^{exp}$, or decreased if $c_{ij} > c_{ij}^{exp}$. Then one repeats the procedure (starting with point 2.)

In practice, we used the couplings J_{ij} and fields h_i obtained from our inference algorithm, based on the large fields expansion, as an educated guess for the initial values of the learning procedure. This starting point is already very close to the true set of couplings and fields, and allows the learning procedure to converge much faster than if it were started from randomly chosen initial values. Figure 1 shows the quality of reconstruction of the correlations c_{ij} and the firing probabilities p_i for the 32 cells common to Flicker and Dark recordings after the Boltzmann-learning algorithm. This figure clearly shows that the couplings and fields found by the learning procedure are the correct ones.

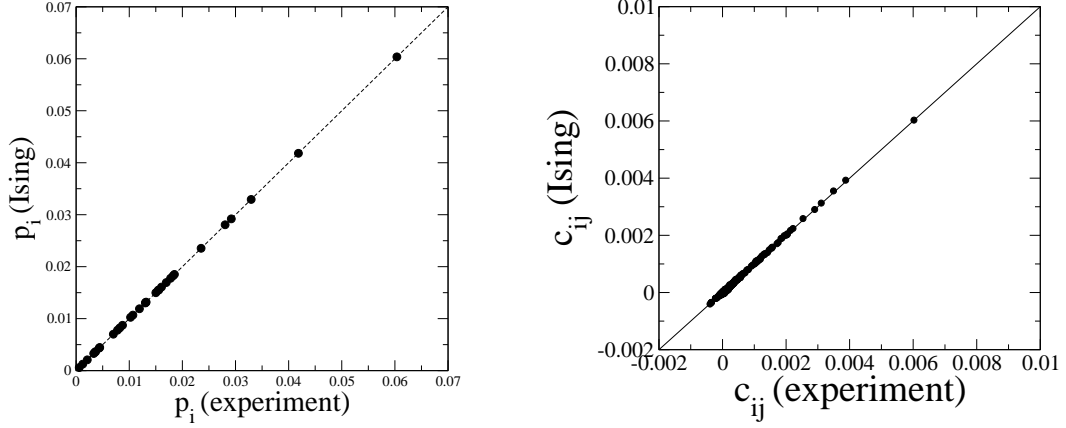


FIG. 1: Comparison of firing probabilities p_i (left) and correlations c_{ij} (right) found through the learning procedure with their experimental values. Results are shown for $N = 32$, $\Delta t = 20$ ms, and Flicker stimulus. Note that the correlations measured for $(0, 1)$ spins are 4 times smaller than their counterparts for ± 1 spins used in Ref. [1].

Figure 2 compares, for every pair i, j , the coupling J_{ij} found by our algorithm with the expansion up to the order $k_{max} = 5$ vs. the value obtained from the learning algorithm for $\epsilon = .0001$. The error bars for the inferred couplings, due to the finite amount of data, are also depicted (see the previous section in Supporting Information). For all three stimuli and Δt ranging from 5 to 20 ms, and for almost all pairs of cells, the discrepancy between the values of the coupling J_{ij} calculated with our algorithm and with the learning procedure is smaller than the uncertainty due to the finite size of the data set. This result confirms the high accuracy of our algorithm.

The algorithm with $k_{max} = 5$, and $N = 32$ runs in a couple of minutes on a personal computer. The running time increases with the number of cells as N^5 , from about 0.4 sec, for $N = 10$, to about 1 hour, for $N = 60$.

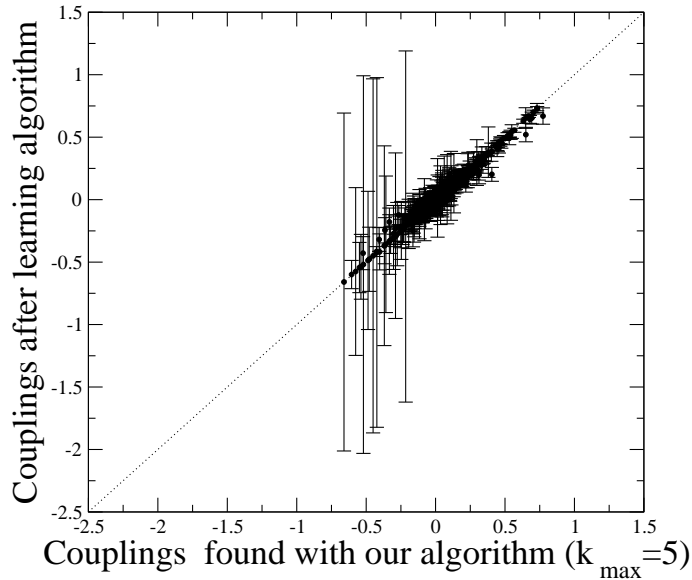


FIG. 2: Comparison of couplings J_{ij} found by the Ising inference with their values after running a Boltzmann-learning algorithm. Results are shown for $N = 32$, $\Delta t = 20$ ms, and Flicker stimulus. The error bars show the uncertainty on the couplings due to the finite sampling. The dashed line represents the $y = x$ line.

IV. CALCULATION OF THE ERROR ESTIMATES FOR THE INFERRED PARAMETERS

We now report how the errors for the inferred fields and couplings, due to the finite sampling, can be calculated. We assume for the moment that the data are generated from an Ising model (4) with given fields $\{h_i\}$ and couplings $\{J_{kl}\}$. The probability of inferring from such data a set of fields $\{h'_i\}$ and couplings $\{J'_{kl}\}$ is then proportional to $\exp(-B S_M[\{h'_i\}, \{J'_{ij}\}])$. When B is very large this probability is strongly concentrated around the values corresponding to the minimum of S_M , i.e. around $\{h_i\}, \{J_{kl}\}$. The difference between the inferred and the true fields and couplings is encoded in the $N(N+1)/2$ -dimensional vector with components $(\{h'_i - h_i\}, \{J'_{kl} - J_{kl}\})$; the distribution of such vectors is asymptotically Gaussian, with a covariance matrix equal to the inverse of the Hessian matrix \mathbf{H}_M of S_M (over B). The existence of this Gaussian distribution is a central result of asymptotic Bayesian inference, where \mathbf{H}_M is called Fisher information matrix.

In order to calculate \mathbf{H}_M we proceed in two steps. We first calculate the Hessian matrix \mathbf{H} of the Ising entropy S (6) by noticing that the entries of \mathbf{H} are simply related to the multi-spin correlations of the Ising model,

$$\mathbf{H} = \begin{pmatrix} \frac{\partial^2 S}{\partial h_i \partial h_{i'}} & \frac{\partial^2 S}{\partial h_i \partial J_{k'l'}} \\ \frac{\partial^2 S}{\partial h_{i'} \partial J_{kl}} & \frac{\partial^2 S}{\partial J_{kl} \partial J_{k'l'}} \end{pmatrix} = \begin{pmatrix} 4 (\langle s_i s_{i'} \rangle - \langle s_i \rangle \langle s_{i'} \rangle) & 8 (\langle s_i s_{k'} s_{l'} \rangle - \langle s_i \rangle \langle s_{k'} s_{l'} \rangle) \\ 8 (\langle s_{i'} s_k s_l \rangle - \langle s_{i'} \rangle \langle s_k s_l \rangle) & 16 (\langle s_k s_l s_{k'} s_{l'} \rangle - \langle s_k s_l \rangle \langle s_{k'} s_{l'} \rangle) \end{pmatrix}, \quad (12)$$

where $\langle \cdot \rangle$ denotes the average with the Gibbs measure (3). Once \mathbf{H} is known, we obtain \mathbf{H}_M by adding $\Gamma \times \text{Identity}$, see (7), and invert \mathbf{H}_M with standard linear algebra routines.

The only difficulty is, therefore, to calculate the multi-spin correlations in (12). In principle, one should infer the couplings and fields, check through Monte Carlo simulations that the experimental magnetizations and correlations are correctly reproduced, and use the same simulations to calculate the entries of \mathbf{H} . In practice, we obtain an excellent and time-inexpensive approximation to \mathbf{H} by computing the correlations directly from the data. The error bars obtained from the two procedures are very similar.

Figure 2 shows the statistical uncertainty associated with the inferred couplings for the Flicker data set. Ten pairs (over 496) of cells have very large error bars $\simeq 2$. As discussed in Section I these pairs of cells never spike together within the data set, and their couplings would be thus minus infinity if it were not for the regularizing term proportional to Γ in (7), see formula (36) in Supporting Information 4. These pairs correspond to localized zero modes of \mathbf{H} , and the error bars on their couplings are equal to the *a priori* standard deviation σ . The other couplings in Fig. 2 have a statistical error much smaller than σ , and are not affected by the value of the parameter Γ .

Figure 3 shows the histograms of the couplings for the 32 cells common to the Flicker and Dark recordings. The full black histograms corresponds to reliable couplings *i.e.* the couplings with relative error smaller than 30%. Note that the absolute values of most unreliable couplings are small, and are compatible with the zero value.

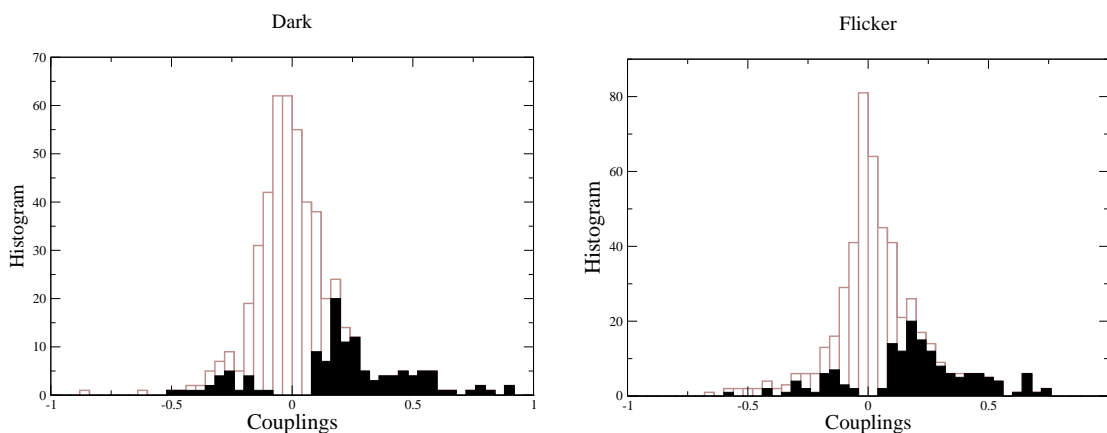


FIG. 3: Histogram of couplings J_{ij} for $N = 32$, $\Delta t = 20$ ms, and Dark and Flicker stimulus. The couplings for which the relative sampling uncertainty is smaller than 30% are black (called reliable) and others (unreliable) in brown.

Supporting Information Appendix, Section 2:

Limitations of the inverse Ising model: higher-order cell correlations and couplings

The inverse Ising model is well suited to reproduce the cell average activities and pair correlations. We can test the quality of this representation of the cellular activities by comparing the higher order correlations extracted from experiments to the predictions obtained from the Ising model.

Let $s_i = 1$, if the neuron i fires at least once in the given time-bin and $s_i = 0$, otherwise. We consider

$$p_{ijk}^{Experiment} = \langle s_i s_j s_k \rangle_{Experiment} \quad (13)$$

where the average is performed over the recorded data: this is the experimental probability that the triplet of cells (i, j, k) fire together in a single time-bin. We also consider the quantity:

$$p_{ijk}^{Ising} = \langle s_i s_j s_k \rangle_{Ising} \quad (14)$$

where the average is now taken over the Ising Gibbs measure, with fields and 2-spin couplings found through the maximum entropy principle (not taking into account 3-spin correlations). To be more precise, given the number N of cells, the bin width Δt , and the stimulus, we first calculate the firing probabilities of the single cells, p_i , and of the pairs of cells, p_{ij} ; we then deduce the Ising couplings and fields, and finally we calculate the probability of triplets (14) with Monte Carlo simulations.

In order to test the validity of the Ising representation, we then compare, for each triplet of cell (i, j, k) , the 3-cell connected correlations:

$$c_{ijk} = p_{ijk} - p_i p_{jk} - p_j p_{ik} - p_k p_{ij} + 2 p_i p_j p_k, \quad (15)$$

obtained from the experiments and via the Ising model inference. The outcome is depicted in Figure 4 for the Flicker and Natural Movie stimuli. For both stimuli, there is a good correlation between the predicted and measured values of c_{ijk} , even though the Ising 3-cell correlations are systematically larger than the experimental ones.

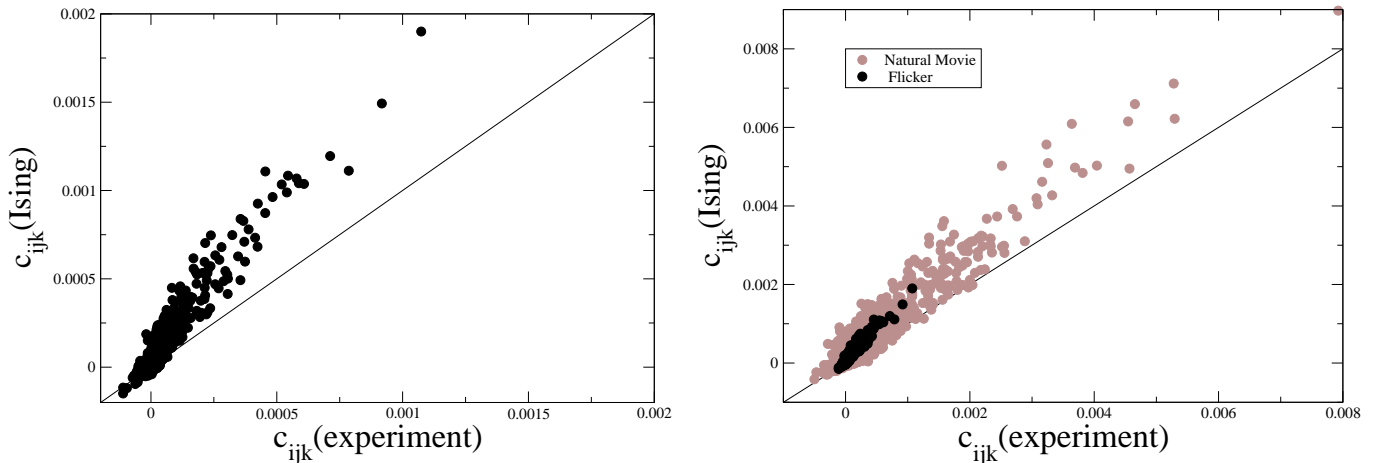


FIG. 4: 3-cell connected correlation c_{ijk} predicted from the Ising model (y axis) compared to their experimental values (x axis) for Flicker (left, $N = 32$ cells) and Natural Movie (right, $N = 40$ cells). Results are shown for $\Delta t = 20$ ms. The 3-cell correlation for Flicker are reported in the Natural Movie panel for comparison.

One can match the predicted and experimental values of the firing activity correlations, if one introduces higher-order couplings between the cells. Indeed, let us consider a new 3-cell contribution

$$E^{(3)} = -8 \sum_{i < j < k} J_{ijk} s_i s_j s_k \quad (16)$$

which we add to the energy E of the Ising model, Eq.(5). We can calculate the 3-cell couplings J_{ijk} within linear response theory, which is asymptotically correct for vanishing differences between $p_{ijk}^{Experiment}$ (13) and p_{ijk}^{Ising} (14). Within the linear response theory:

$$J_{ijk} = \frac{1}{8} \sum_{i' < j' < k'} [M^{-1}]_{ijk, i'j'k'} (p_{i'j'k'}^{Experiment} - p_{i'j'k'}^{Ising}), \quad (17)$$

where M^{-1} denotes the inverse matrix of the multi-spin susceptibility

$$M_{ijk, i'j'k'} = \langle s_i s_j s_k s_{i'} s_{j'} s_{k'} \rangle_{Ising} - \langle s_i s_j s_k \rangle_{Ising} \langle s_{i'} s_{j'} s_{k'} \rangle_{Ising}. \quad (18)$$

In practice, the elements of the M matrix are calculated through Monte Carlo simulations of the Ising model. The resulting 3-cell couplings are depicted in Fig. 5 for Flicker stimuli (qualitatively similar results are also obtained for Dark and Natural Movie stimuli, with a higher probability for triplets in the latter case). It is useful to note here that:

- the 3-cell couplings J_{ijk} corresponding to the triplets of cells (i, j, k) firing often together, *i.e.* those with large $p_{ijk}^{Experiment}$, are small (in absolute value) compared to the 2-cell couplings in the Ising model. In other words, the difference between the experimental and Ising values for the 3-cell connected correlations, though visible in Fig. 4, can be corrected by adding a small 3-cell coupling.
- on the contrary, the couplings associated with triplets of cells that are rarely active simultaneously, may take any finite value. Note, however, that the linear response theory cannot be quantitatively trusted for too large (absolute) values of the couplings.

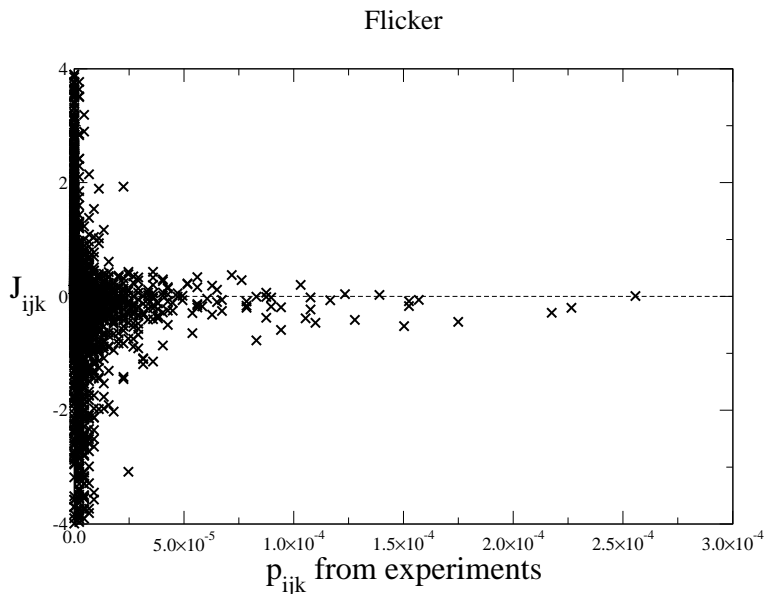


FIG. 5: Three-spin couplings J_{ijk} obtained through the linear response theory, as a function of the triplet-firing probability $p_{ijk}^{Experiment}$. These results were obtained for $N = 32$ cell, $\Delta t = 10$ ms, and the Flicker stimulus. Similar results can be obtained for Dark.

The discrepancy between the experimental and the Ising values for the 3-cell connected correlations shown in Fig. 4 is a delicate issue from the numerical point of view. Our Ising prediction for c_{ijk} are indeed marred with

numerical errors coming from the Monte Carlo simulations. To avoid this problem, we have looked at small subsets of $n = 10$ neurons, for which the firing probabilities and correlations can be calculated exactly from the knowledge of the couplings and fields. With our inference algorithm, keeping clusters with $k_{max} \leq 7$ spins, we have found the couplings and fields reproducing the firing probabilities p_i and p_{ij} within 10^{-5} for the first ten cells of the Flicker data set. We have then calculated the 3-cell connected correlations; the outcome is shown in Fig. 6. As in Fig. 4, the Ising predictions for the large correlations are generally higher than the experimental values. This result seems to be independent of the time-bin width Δt (Figure 6).

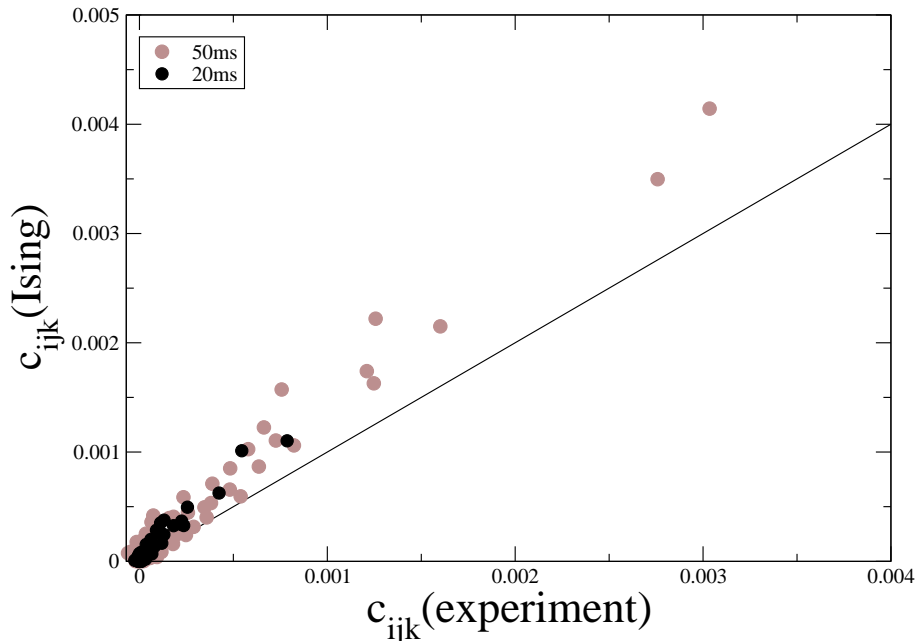


FIG. 6: 3-cell connected correlation c_{ijk} predicted from the Ising model (y axis) compared to their experimental values (x axis) for the first ten cells of the Flicker data set, and two bin widths $\Delta t = 20, 50$ ms. The values found for c_{ijk} for the first 120 triplets of cells are very similar to the one calculated from the whole set of 32 cells in Figure 4 (left).

In conclusion, we find that the Ising model representation of the spiking activities (defined with 2-cell couplings J_{ij} only) is good for the most likely configurations, while rare events require the introduction of higher order multi-cell couplings. Whether the latter result is due to a failure of the Ising representation or to the insufficient sampling of the tail of the activity distribution remains unclear.

We can thus clarify the reasons underlying the success of the Ising model representation. For Dark stimulus, for instance, if we consider all $N = 60$ recorded cells (and not only the 32 cells shared with the Flicker recordings) and take $\Delta t = 20$ ms, we then have at our disposal $B \simeq 10^5$ experimental configurations to sample the space of total $2^N \simeq 1.15 \times 10^{18}$ configurations. Since the sampled configurations $\mathbf{s} = \{s_1, s_2, \dots, s_N\}$ are far from being uniformly distributed, the entropy

$$S = - \sum_{\mathbf{s}} p(\mathbf{s}) \log_2 p(\mathbf{s}) \quad (19)$$

is smaller than N . In practice, we estimate $S \simeq 4.42$ bits. Hence the number of 'effective' configurations is

$$\mathcal{N}_{eff} = 2^S \simeq 21.5 . \quad (20)$$

It is thus not surprising that a good fit of the frequencies of those configurations can be obtained with only $N \times (N + 1)/2 = 1830$ degrees of freedom (the number of the 2-cell couplings J_{ij} and the fields h_i in the Ising representation). This argument holds also for Flicker stimuli: $S \simeq 3.29$ bits for $N = 51$ cells.

To test the quality of the representation of rare configurations, we can also consider the probability $P(k)$ that k cells are active in the same time-bin. The results are shown in Fig. 7 for the Flicker stimulus (similar results are

obtained for Dark). The agreement is good for small k , and worsens as the number of simultaneously active cells increases. This finding strengthens the conclusion that rare events are not adequately taken into account by the Ising representation. Notice that in Ref. [1] a better agreement between the experimental and calculated $p(k)$ was indeed found for Natural-Movie, a structured stimulus for which the global activity is higher than in Flicker or in Dark.

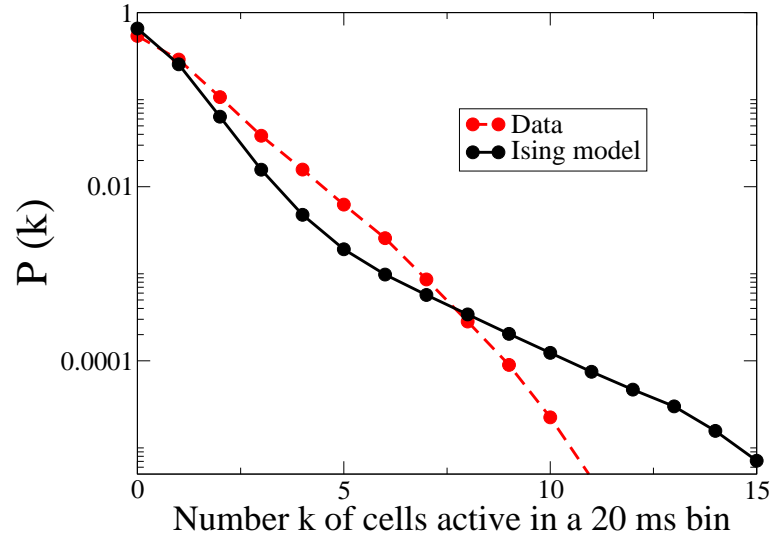


FIG. 7: Probability that k cells are active in the same time-interval bin calculated from the Ising model and experimental data. Results are shown for Flicker and $\Delta t = 20$ ms. Events with probabilities of the order of, or smaller than, $1/B \simeq 2 \cdot 10^{-5}$ cannot be sampled from the data set.

Supporting Information Appendix, Section 3:

Algorithm for the Inverse Integrate-and-Fire Problem

The Leaky Integrate-and-Fire (LIF) model is defined in the Methods section of the main paper. In the following the equations (4), (5), (6) in the main paper will be referred to as, respectively, (M4), (M5), and (M6).

For given values of the couplings G_{ij} and of the average currents I_i , equations (M4,M5,M6) implicitly express the likelihood $P[\{t_{i,k}\}|\{G_{ij}, I_i\}]$ that the population of N neurons emit spikes at times $\{t_{i,k}\}$, as a product of first-passage times (FPT) probabilities [20]:

$$P[\{t_{i,k}\}|\{G_{ij}, I_i\}] = \prod_{i,k} P_{FPT}[t_{i,k+1}|\{G_{ij}, I_i\}, \{t_{j,l} < t_{i,k+1}\}, t_{i,k}]. \quad (21)$$

The (i, k) term in the product denotes the probability that the potential of cell i , starting from the zero value at time $t_{i,k}^+$, will reach the threshold value for the first time at $t_{i,k+1}^-$, given the values of the currents, of the couplings and of all firing times $t_{j,\ell} \in [t_{i,k}, t_{i,k+1}]$ of spikes by other cells. To lighten notations, we will omit below the dependence on firing times in P_{FPT} , and write only the explicit dependence on couplings and currents. Each one of the first-passage time probabilities can be expressed as a path-integral over the time-traces of the potentials,

$$P_{FPT}[t_{i,k+1}|\{G_{ij}, I_i\}] = -\frac{d}{dt_{i,k+1}} \int_{V_i(t_{i,k})=0}^{V_i(t_{i,k+1})<1} DV_i(t) \exp\left[-\frac{A[V_i(t)|\{G_{ij}, I_i\}]}{2\sigma^2}\right] \quad (22)$$

with

$$A[V_i(t)|\{G_{ij}, I_i\}] = \int_{t_{i,k}}^{t_{i,k+1}} dt \left(\frac{dV_i}{dt}(t) + g V_i(t) - I_i^{syn}(t) - I_i \right)^2 \quad (23)$$

The integration domain in (22) is restricted to sub-threshold potential $V_i(t) < 1$, $\forall i, t$. The boundary conditions are $V_i(t_{i,k}) = 0$, while the integral is performed over all possible values $V_i < 1$ of the potential at time $t_{i,k+1}$.

In principle, the path-integral (22) can be calculated by solving many Fokker-Planck equations, one for each spike in the data set, associated to one-dimensional Ornstein-Uhlenbeck processes with moving boundaries [7, 11]. In practice, however, this approach is inadequate to deal with the data sets consisting of hundreds of thousands of spikes. We have, therefore, resorted to an approximation for P , which is asymptotically exact when the amplitude σ of the synaptic noise (M6) tends to zero. Indeed, for small σ the path integral (22) is dominated by the contribution coming from a single path for the potential, called the classical path in physics [8] and the optimal path in large deviation theory [9]. The optimal potential, hereafter referred to as $V_i^*(t)$, is simply the one minimizing the action A [10] with the boundary conditions:

$$V_i(t_{i,k}^+) = 0 \quad \text{and} \quad V_i(t_{i,k+1}^-) = 1. \quad (24)$$

The outcome of the minimization of A can be written as follows:

- Let us assume first that $V_i^*(t) < 1$. Then, the functional derivative of A , eq. (23), with respect to $V_i^*(t)$ must vanish, which gives

$$-\frac{d^2 V_i^*}{dt^2}(t) + g^2 V_i^*(t) + \frac{dI_i^{syn}}{dt}(t) - g I_i^{syn}(t) - g I_i = 0. \quad (25)$$

We now turn this second order differential equation for the optimal potential into a first order differential equation at the price of introducing a new function, $\eta_i^*(t)$, and a new first order differential equation for this function. It is straightforward to check that the solution of

$$\frac{dV_i^*}{dt}(t) = -g V_i^*(t) + I_i^{syn}(t) + I_i + \eta_i^*(t) \quad (26)$$

is a solution of the optimization equation (25) provided $\eta_i^*(t)$ fulfills

$$\frac{d\eta_i^*}{dt}(t) = +g \eta_i^*(t) . \quad (27)$$

Note the change of sign in front of g in (27) with respect to (26) [8].

The similarity between equations (M4) and (26) allows us to interpret $\eta_i^*(t)$ as a current noise. However, this noise is no longer stochastic, but rather it follows the deterministic path solution of eq. (27). We will, therefore, in the following refer to $\eta_i^*(t)$ as the optimal noise. Solving (27) shows that the noise term is an exponential of the type

$$\eta_i^*(t) = \eta_i^c \exp(gt), \quad (28)$$

where η_i^c is a constant, provided that the potential remains below the threshold.

- It may happen that the optimal potential only touches the threshold without actually crossing it at intermediate times. When this is the case, the optimal potential equals $V_i^*(t) = 1$ and its derivative with respect to the time vanishes. The value for the optimal noise can be then calculated from Eq. (26), with the result

$$\eta_i^*(t) = g - I_i^{syn}(t) - I_i . \quad (29)$$

This equation merely gives the value, which the noise has to take, for the potential to remain at the threshold (without crossing it).

The set of the coupled equations (26), (28) and (29) cannot be solved directly due to the interplay between the sub-threshold and threshold regimes. There exists, however, an efficient solving procedure for the case of the synaptic integration times, t_s , much smaller than the membrane characteristic time $1/g$. In this case, the noise coefficient η_i^c in (28) can change its value at discrete times, coinciding with the instants of the input spikes only. At these isolated 'contact points', the potential reaches the threshold (without crossing it). A detailed study of the dynamical equations (M4) and (28,29) shows that, in the $t_s \rightarrow 0$ limit, the noise $\eta_i^*(t_c^+)$ assumed immediately after a contact point at time t_c , can take any value larger than its value $\eta_i^*(t_c^-)$ assumed immediately before t_c . Such simple contact rule suggests a fast procedure to determine the optimal noise path. For the sake of simplicity, we now describe this procedure for the case of $g = 0$ only, although it should be stressed that it can easily be adapted for non-zero g values as well.

Let $t_1 < t_2 < \dots < t_L$ be the times of the spikes received by the cell i between its own two successive spikes, emitted at times $t_0 \equiv t_{i,k} (< t_1)$ and $t_{L+1} \equiv t_{i,k+1} (> t_L)$. Let us call J_l the value of the coupling from the cell emitting a spike at time t_l to the cell i . We calculate, for each $l = 1, 2, \dots, L + 1$ the value of the noise coefficient $\eta_i^c(t)$ such that the solution of (26) matches the boundary conditions $V_i(t_{i,k}) = 0$ and $V_i(t_l) = 1$, if the coupling J_l is negative, $V_i(t_l) = 1 - J_l$, if J_l is positive. By taking now the smallest noise coefficient, obtained for, say, $l = l_0$, we obtain the optimal potential and noise in the time interval $[t_0; t_{l_0}]$. The procedure can now be iterated to determine the optimal paths for the potential and the noise in a next time interval $[t_{l_0}; t_{l_1}]$, with $l_1 > l_0$ [21], and so on, until completion of the whole inter-spike interval $[t_0; t_{L+1}]$. The procedure is then repeated for all the inter-spike intervals of the cell i . An example of optimal paths for the noise and potential is shown in Figure 8.

Once we have determined the optimal noise (and potential) of cell i , for a given set of couplings G_{ij} and currents I_i , we can obtain the *a posteriori* probability for the latter from the Bayes formula

$$P[\{G_{ij}, I_i\} | \{t_{j\ell}\}] = P[\{t_{j\ell}\} | \{G_{ij}, I_i\}] \times P_0[\{G_{ij}, I_i\}] / P_1[\{t_{j\ell}\}] = \exp \left[-\frac{1}{2\sigma^2} \sum_k (A[V_i^*(t) | \{G_{ij}, I_i\}] + o(1)) \right] \quad (30)$$

in the small σ limit, where the sum runs over the spikes emitted by cell i . The couplings and currents with maximal probability are the one maximizing the likelihood $-A[V_i^*(t) | \{G_{ij}, I_i\}]$ (23). As A is clearly a convex function of G_{ij} and I_i [11] its minimum is easily found through the gradient descent or Newton-Raphson method. As in the Ising model case the knowledge of the Hessian matrix of A gives access to the uncertainty (error bars) on the couplings and currents.

It is important to note that the small σ approximation made here is actually quantitatively reliable even for finite noise variances. Let us consider the (small) contribution to the first-passage time probability coming from paths close to, but not coinciding with the optimal path. Such a close path for the potential can be expressed as $V_i^*(t) + \delta V_i(t)$, where $\delta V_i(t)$ is the deviation from the optimal potential of the cell i at time t . Here $\delta V_i(t_{i,k}) = \delta V_i(t_{i,k+1}) = 0$ in

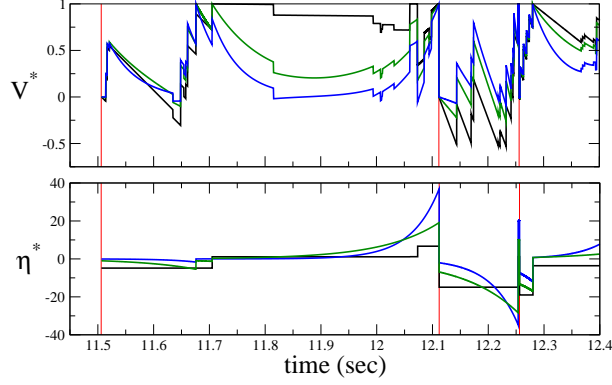


FIG. 8: Optimal potential and noise for the first cell of the Flicker data set for $g = 0$ (black line), $g = 10 \text{ sec}^{-1}$ (green line) and $g = 20 \text{ sec}^{-1}$ (blue line). Only two inter-spike intervals (delimited by the red edges) are shown, during which the cell receives 20 and 10 (in the first and the second interval, respectively) inputs from the other 31 cells. The number and the locations of the contact points depend on the value of g . For $g = 0$ there are 3 contact points, corresponding to 4 increasing steps in the noise, and 4 slopes of the potential. The couplings J_{1j} and current I_1 are set to their most likely values for $g = 0$.

order to satisfy the boundary conditions (6). The corresponding action is equal to the optimal action plus a positive increment,

$$\delta A = \int_{t_{i,k}}^{t_{i,k+1}} dt \delta V_i(t) \left(-\frac{d^2}{dt^2} + g^2 \right) \delta V_i(t). \quad (31)$$

Integrating over these paths generates an additive correction of the order of σ^2 to the optimal action A in the exponential on the right hand side of (30). The key point is that this correction does not depend on the couplings and currents as can be seen from (31), and is therefore irrelevant for the inverse problem.

Our I&F model can also be made more realistic by taking into account the refractory period present in real neurons. To do this, we discard the inputs received by a neuron during a delay t_r after a spike emission. In practice, t_r is of the order of a few ms, and is much smaller than the typical inter-spike interval. In consequence, the couplings inferred with or without the refractory period are very similar. However, the presence of a refractory period is important for a simulation of the I&F model, see Supporting Information 4.

Supporting Information Appendix, Section 4:

On Cross-correlograms: Analysis of Data, Relationship with Couplings, and Simulations

We compare here the correlation index introduced in the analysis of cross-correlograms [12] and the effective couplings calculated within the inverse Ising model framework. Section I goes over the definition of the correlation index. The relationship with couplings J_{ij} is explained in Section II. We then study the dependence of correlation indices and couplings upon stimuli (Section III) and the width Δt of time-interval bins (Section IV). The cross-correlograms obtained from the Integrate-and-Fire model are compared to the experimental measures in Section V.

The cells are numbered from 1 to 32 in Dark and Flicker data sets. The pairs of cells denoted by a, b, c, d in the main paper correspond to, respectively, pairs 5-17, 3-18, 11-26, 1-22.

I. DEFINITION OF THE CORRELATION INDEX

The cross-correlogram for the cells i and j is the histogram of the delays between their spiking times,

$$H_{ij}(\tau) = \frac{T}{N_i N_j} \sum_{a,b} \delta(\tau - t_{j,b} + t_{i,a}) . \quad (32)$$

Here N_i and N_j represent the number of spikes emitted by the cells i and j , respectively, and T is the total duration of the recordings. As before, $t_{i,a}$ is the time of emission of the a^{th} spike of cell i , $a = 1, 2, \dots, N_i$. Examples of cross-correlograms for various pairs of neurons and for both Dark and Flicker stimuli are shown in Figure 2 of the main text.

We observe that $f_j \times H_{ij}(\tau)$ can be interpreted as the instantaneous firing rate of the cell j at time τ , conditioned on the existence of a spike of the cell i at time 0. Based on the cross-correlogram H_{ij} one can define the cross-correlation index (CI) on time-scale τ :

$$CI_{ij}(\tau) = \frac{1}{\tau} \int_{-\tau/2}^{\tau/2} d\tau' H_{ij}(\tau') . \quad (33)$$

$CI_{ij}(\tau)$ is the number of spikes emitted by the cells i and j with a delay smaller than $\tau/2$ (in absolute value), divided by the number of times the two cells would fire in the same time window if they were independent. Note that when the cross-correlogram is flat around the origin, then the integral in (33) grows linearly with τ , and the correlation index remains constant.

Consider now a binning of the emission times of width Δt much smaller than the typical inter-spike intervals of single cells. The probability that the cell i emits a spike in a given bin is $p_i \simeq f_i \times \Delta t$, where f_i is the firing rate; the joint probability that the pair of cells (i, j) both emit a spike in the same bin is $p_{ij} = CI_{ij}(\Delta t) \times p_i \times p_j$, where this last equality follows from the definition of the correlation index. Hence

$$CI_{ij}(\Delta t) = \frac{p_{ij}}{p_i p_j} . \quad (34)$$

We stress that this equality is correct when each cell is likely to emit at most one spike in a single time-interval bin.

II. CONNECTION BETWEEN CORRELATION INDEX AND COUPLINGS

As sketched in Supporting Information 1 the couplings can be systematically expanded in powers of the connected correlation $c_{ij} = p_{ij} - p_i p_j$ with the following results:

- to the lowest order (linear) in the expansion one finds

$$J_{ij} \simeq \frac{c_{ij}}{4 p_i p_j} = \frac{1}{4} (CI_{ij}(\Delta t) - 1) . \quad (35)$$

This expression coincides with the Hebb's rule for learning synaptic coefficients from correlated spiking activities.

- if we sum all the contributions (to any power) including c_{ij} only, and discards all the terms including correlation between other cells, we find the 2-cell approximation for the couplings. For small Δt (or more precisely when p_i and p_j are small):

$$J_{ij}^{2-cell} \simeq \frac{1}{4} \log \left(CI_{ij}(\Delta t) - \frac{\Gamma J_{ij}^{2-cell}}{p_i p_j} \right) \quad (36)$$

This self-consistent equation simplifies to

$$J_{ij}^{2-cell} \simeq \frac{1}{4} \log CI_{ij}(\Delta t) , \quad (37)$$

when $CI_{ij}(\Delta t) \gg \Gamma p_i p_j$, i.e. when the frequency of occurrence of the simultaneous spiking of the two cells is non-zero in the experimental data set. For pairs that never spike together in a time-bin Δt the presence of the factor Γ prevents the coupling to be minus infinite, see Supporting Information 1. Expression (37) coincides with the ‘synchrony index’ defined in [13]. A generalization of the 2-cell approximation, valid for large Δt , can be obtained from equation (10) of Supporting Information 1. The 2-cell formula (37) provides a very accurate approximation for the couplings of some pairs of cells, such as 5 and 17, see Figure 1A in the main paper.

- Larger orders of the diagrammatic expansion provide the coupling J_{ij} as a global function not only of c_{ij} , but also of correlations c_{kl} , with $k \neq i$ or $l \neq j$. Network contributions c_{kl} are for example important for cells 3 and 6 in Figure 1B (main paper): these cells have a positive coupling $J_{3,6}$, and are both strongly coupled to cells 1 and 21. The indirect interactions between cells 3 and 6 through cells 1 and 21 are responsible for a substantial fraction of the correlations between cell 3 and 6. As a consequence, coupling $J_{3,6}$ cannot be accurately approximated by the 2-cell approximation (37). Network contributions are even more important in the case of Figure 1C (main paper): the direct coupling between cells 1 and 22 is negative, while their correlation is positive due to indirect strong interactions through cells 6 and 27.

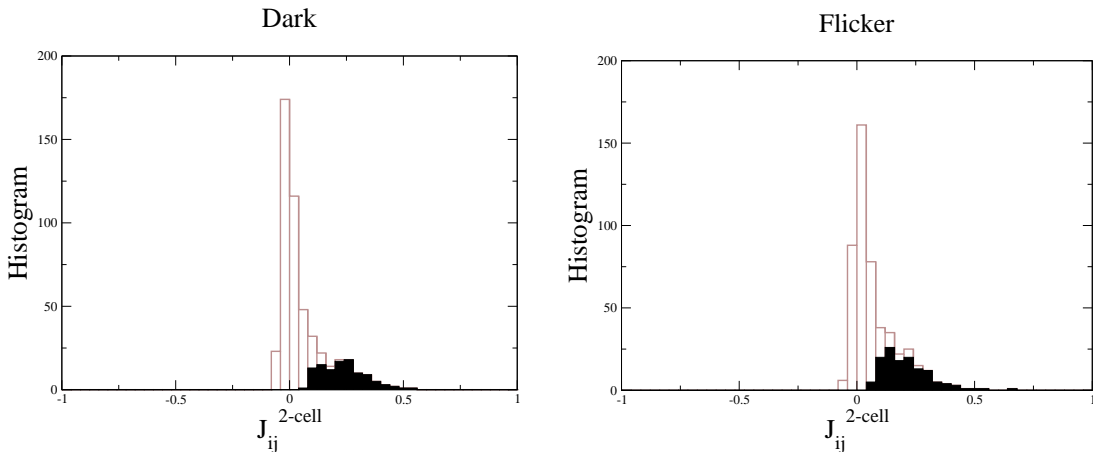


FIG. 9: Histogram of the two-cell approximation to the couplings J_{ij}^{2-cell} for $N = 32$, $\Delta t = 20$ ms, and Dark and Flicker stimuli. Black/brown values correspond to reliable/unreliable couplings *i.e.* with relative errors smaller/larger than 30%.

The histograms of J_{ij}^{2-cell} in Fig. 9 can be compared to the histograms of J_{ij} in Fig. 3 for Flicker and Dark data. The main difference is the absence of negative-valued couplings in the 2-cell couplings histograms, apart for some weakly negative and unreliable interactions.

To assess the accuracy of the 2-cell approximation more precisely, we show in Figure 10 the difference $\frac{1}{4} \log CI_{ij} - J_{ij}$ versus the value of the couplings, J_{ij} . The 2-cell approximation is relatively accurate for large positive couplings, while it is generally bad for negative couplings. Negative couplings seem to be more sensitive to network effects and thus not directly noticeable from the knowledge of the correlation index.

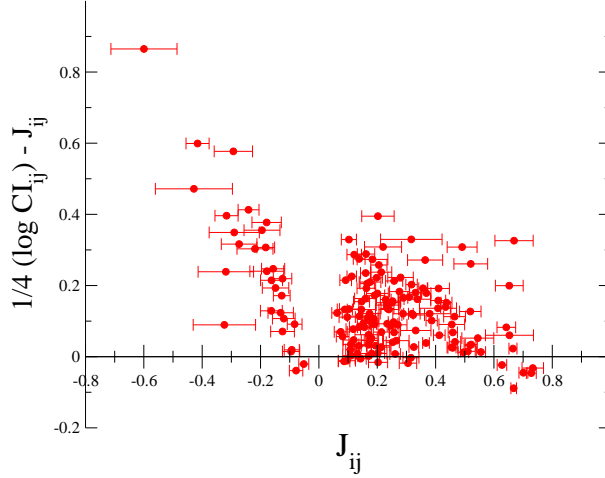


FIG. 10: Difference $J_{ij}^{2-cell} - J_{ij}$ as a function of J_{ij} for Flicker recordings. Only pairs with reliable interactions are shown. Here $\Delta t = 20$ ms. Error bars on J_{ij} are shown along the horizontal axis.

III. CONSERVATION OF CORRELATION INDICES UNDER DIFFERENT STIMULI

Principle component analysis has been used in our study to show that some couplings are conserved under a change of stimulus, see Figure 2 in the main text for details. We repeat the same analysis here for pair-wise correlations $c_{ij} = p_{ij} - p_i p_j$ and correlation indices:

- Pair-wise correlations (Figure 11): we calculate the three correlation coefficients

$$\begin{aligned}
 \langle c^D c^D \rangle &= \frac{1}{496} \sum_{i < j} c_{ij}^D \times c_{ij}^D \\
 \langle c^D c^F \rangle &= \frac{1}{496} \sum_{i < j} c_{ij}^D \times c_{ij}^F \\
 \langle c^F c^F \rangle &= \frac{1}{496} \sum_{i < j} c_{ij}^F \times c_{ij}^F
 \end{aligned} \tag{38}$$

where the subscripts D, F stand for Dark, Flicker. The sums run over the $32 \times 31/2 = 496$ pairs of cells. We then diagonalize the covariance matrix

$$M = \begin{pmatrix} \langle c^D c^D \rangle & \langle c^D c^F \rangle \\ \langle c^D c^F \rangle & \langle c^F c^F \rangle \end{pmatrix}. \tag{39}$$

The eigenvectors are $v_1 = (1, 0.52)$ and $v_2 = (1, -1.91)$ with corresponding eigenvalues $\lambda_1 = 9.45 \cdot 10^{-7}$ and $\lambda_2 = 2.14 \cdot 10^{-7}$. The principal axes do not correspond to the $(1, 1)$ and $(1, -1)$ directions as is the case in the analysis of the couplings.

- Correlation indices (Figure 12): the above analysis is repeated for correlation indices $CI_{ij}(\Delta t)$ instead of correlations c_{ij} . The eigenvectors of the correlations matrix are $v_1 = (1, 1.08)$ and $v_2 = (1, -0.92)$ with corresponding eigenvalues $\lambda_1 = 6.00$ and $\lambda_2 = 0.34$. The alignment of the principal axes with the $(1, 1)$, $(1, -1)$ directions is better than in the correlation case, and comparable to the one found in the coupling analysis. The distribution of the CIs is not centered around 0, and the covariance matrix is dominated by pairs of cells with strong positive CIs. These pairs correspond to most of the strong positive couplings, accurately estimated from the 2-cell approximation, see Figure 10. Note that the coupling $J_{3,6}$ in Figure 1B (main paper) is conserved in Flicker and Dark (equal to 0.4 in both cases), while the CI is not: $\frac{1}{4} \log CI = 0.34, 0.48$ in Dark and Flicker, respectively.

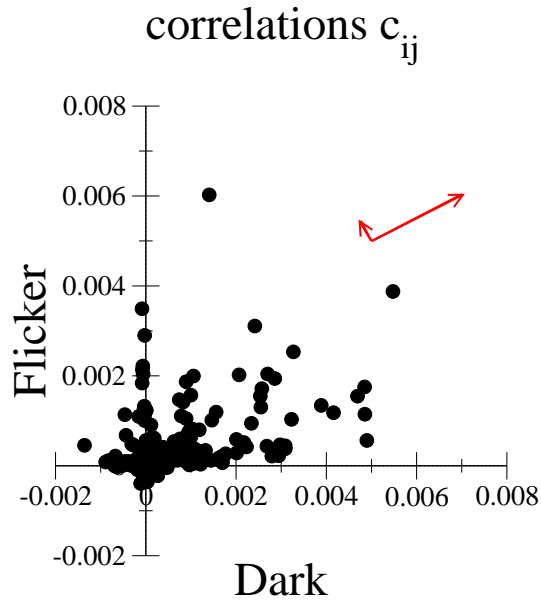


FIG. 11: Connected pairwise correlations c_{ij} in Flicker versus their values in Dark for all pairs of cells (i, j) . The bin-width is $\Delta t = 20$ ms. The red arrows indicate the principal axes v_1, v_2 , with lengths proportional to the eigenvalues λ_1, λ_2 .

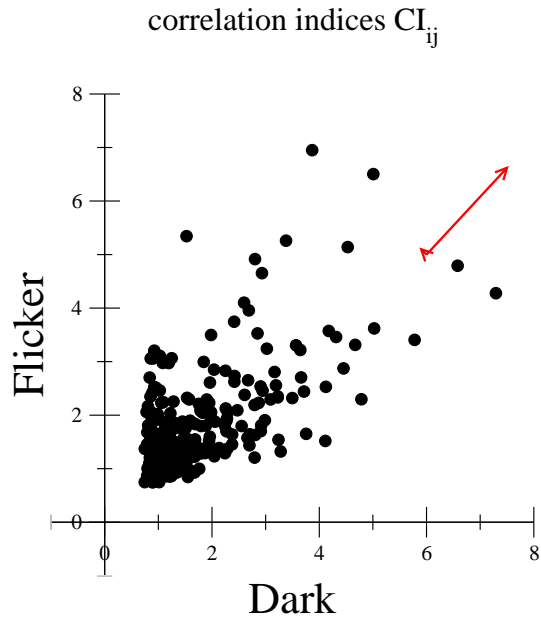


FIG. 12: Correlation indices $CI_{ij}(\Delta t)$ in Flicker versus their values in Dark for all pairs of cells (i, j) . The time scale is $\Delta t = 20$ ms. The red arrows indicate the principal axes v_1, v_2 , with lengths proportional to the eigenvalues λ_1, λ_2 .

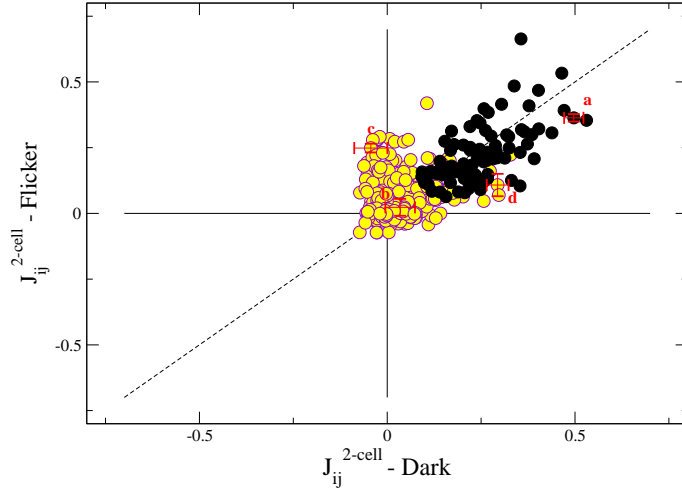


FIG. 13: J_{ij}^{2-cell} in Flicker versus their values in Dark for all pairs of cells (i, j) . The time scale is $\Delta t = 20$ ms. Note that for the positive part this is similar to Fig 2 main text..

Figure 13 shows how correlation indices are conserved in Flicker and Dark conditions. As in Figure 2 of the main text we separate reliable and unreliable 2-cell couplings J_{ij}^{2-cell} , and mark the four pairs a, b, c, d with the error bars. The positive-positive quadrants in Figure 2 of the main text and Fig.13 are similar, *e.g.* see pair a . However, the pairs b, c, d , with negative couplings in Dark and/or Flicker conditions, have larger and reliable values, in the Figure 2 of the main text than in Fig. 13, and are better distinguished and clustered.

IV. COUPLINGS AND CORRELATION INDICES AS FUNCTIONS OF Δt .

The Ising model takes into account only correlations between cells spiking in the same time-bin, of size Δt . Temporal correlations on longer time scales can be taken into account by increasing Δt . Here, we study the behavior of the couplings and correlation indices as a function of Δt ranging from 5 to 50 ms[22], for four representative pairs of cells recorded in Dark and Flicker (shown in Figure 2 of the main text).

Figure 14 shows the correlation indices $CI_{ij}(\Delta t)$ and the couplings $J_{ij}(\Delta t)$ and their 2-cell approximations obtained from the improved formula, valid also at large Δt , for pairs:

- 5-17 (pair a in Figure 2 of the main text): strong coupling conserved in Dark and Flicker;
- 3-18 (pair b in Figure 2 of the main text): negative and conserved in Dark and Flicker;
- 11-26 (pair c in Figure 2 of the main text): positive in Flicker and negative in Dark;
- 1-22 (pair d in Figure 2 of the main text): positive in Dark and negative in Flicker.

For the corresponding cross-correlograms $H_{ij}(\tau)$, see Figure 2 of the main text.

Pair 5-17 is characterized, both in Flicker and Dark, by a peak of half-width of 20 ms in the cross-correlograms. The couplings are large and have small error bars. Couplings are slightly larger in Dark than in Flicker conditions. Coupling values decrease increasing Δt . The 2-cell approximation is very accurate for this pair.

Pair 3-18 is characterized both in Flicker and in Dark by a flat cross-correlogram. For this pair network effects are important; indeed, the 2-cell approximation provides a positive coupling while the real value of the coupling, due to the overall correlations in the network, is negative. Couplings value are quite similar in Flicker and Dark and do not change noticeably with Δt .

Pair 11-26 is characterized by cross-correlogram with a peak in Flicker and a dip of width $\simeq 50$ ms in Dark. The coupling is negative in Dark and positive in Flicker, and reasonably constant, up to $\Delta t = 50$ ms. Although this

coupling is long-range in the receptive fields plane (see Figure 2 in main text) it is very accurately estimated by the 2-cell approximation, and is therefore not influenced by network effects.

Pair 1-22 is characterized by a peak in the cross-correlogram, located off the origin and corresponding to a delay τ (τ is about 40 ms in Flicker and 10 ms in Dark). The coupling starts to increase when Δt exceeds 2τ . The binning size $\Delta t = 20$ ms used in Figure 2 of the main text, is therefore not sufficient to take into account the positive and time-delayed correlation between pair 1 and 22 in Flicker. The resulting coupling is negative in Flicker, while it is positive in Dark where the delay τ is smaller. The 2-cell approximation overestimates the true value of the coupling.

To summarize, couplings that are positive in both Dark and Flicker recordings correspond to cross-correlograms with a strong positive peak. Couplings positive in Dark and negative in Flicker have often cross-correlograms characterized by a larger delay in Flicker than in Dark. Long-range couplings, which are positive in Flicker and negative, or close to zero, in Dark correspond to peaked cross-correlograms in Flicker and to flat or 'bumpy' cross-correlograms in Dark.

V. CROSS-CORRELOGRAMS WITH THE I&F MODEL

In this section we compare the cross-correlograms obtained from the Integrate-and-Fire model to their experimental counterparts. We first infer the I&F couplings and currents for the 32 cells in Dark and Flicker, with dynamical parameters $g = 0$ (no-leaking of the membrane) and $t_s = 0$ (immediate synaptic integration). We then simulate the coupled dynamics of the 32 cells with these inferred couplings and currents and a refractory period $t_r = 5$ ms. The network of the 32 cells is in a state of persistent dynamical activity when the variance of the noise is chosen to be $\sigma^2 = 1$.

In Figure 15 and Figure 16 we compare the correlation histograms obtained from the simulated dynamics with the experimental histograms for the four pair of cells 5-17, 3-18, 11-26, 1-22, both in Dark and Flicker. Generally speaking, the I&F model is able to reproduce the qualitative difference between cross-correlograms with a positive peak and those with a dip at, or close to, the origin. We analyze first the differences between simulations and experiments:

1. *Case of experimental cross-correlograms with a peak centered in $\Delta t = 0$, e.g. pair 5-17 both in Flicker and Dark, pair 11-26 in Flicker only.* The histograms obtained from I&F simulations have a large peak centered at $\Delta t = 0$, which does not spread beyond a window of about 50 ms, as is the case for the experimental data. The reason for this difference is that in the I&F model the synaptic integration time, t_s , vanishes. Therefore, within this model there is no synaptic delay between cells, and correlations in spiking activity are mostly simultaneous.
2. *Case of experimental cross-correlograms with a delayed positive peak, e.g. pair 1-22 in Dark and Flicker.* Again, the I&F model reproduces a positive peak, but not the experimental offset of the cross-correlogram. The reason is the same as in case 1, above. To support our interpretation, we have checked that, both in case 1 and case 2, the correlation index (integral of H , see equation (33)) has similar values for the experiments and the I&F simulations over a time window $\Delta t = 100$ ms.
3. *Case of flat correlograms, e.g. pair 3-18 in Flicker and Dark, and correlograms with a dip, e.g. pair 11-26 in Dark.* These cross-correlograms are well reproduced by the I&F model.

We have also simulated the I&F dynamics of a pair of cells in presence of the *recorded spikes* of the 30 other cells. Figure 17 show that the resulting correlograms are very similar to the ones obtained by the simulation of the whole network of 32 cells. However, the delayed peak of the pair 1-22 is better reproduced; indeed the activity of other cells, being truly experimental, includes delayed correlations.

In conclusion, despite its extreme simplicity and the crude assumptions made about its parameters, the I&F model is capable of reproducing the essential features present in the experimental cross-correlograms.

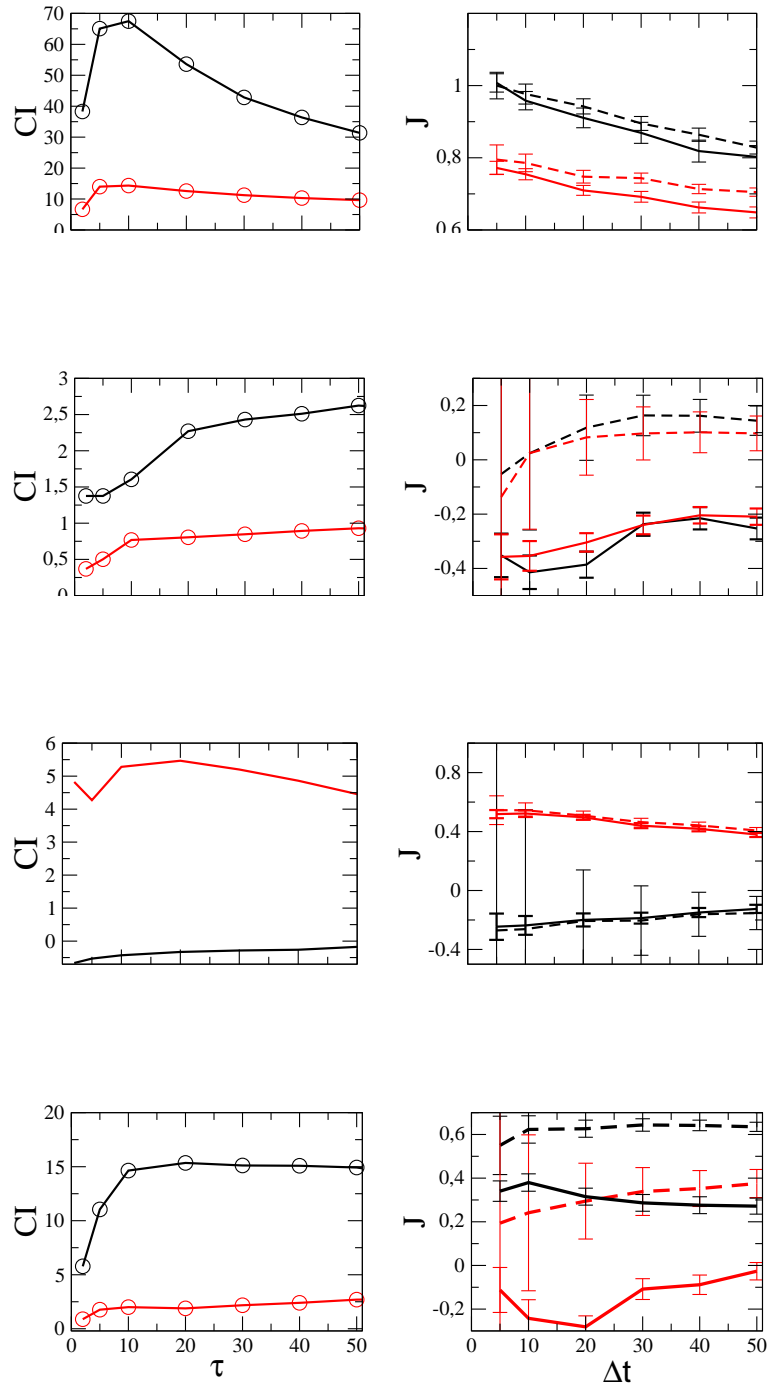


FIG. 14: Left: Correlation index (CI), Right: Couplings (solid line: couplings, dashed line: two cell approximation) for $5 < \Delta t < 50$ ms. Results correspond, from top to down, to pairs 5-17, 3-18, 1-26, 1-22. Dark curves represent Dark stimulus, red curves correspond to Flicker.

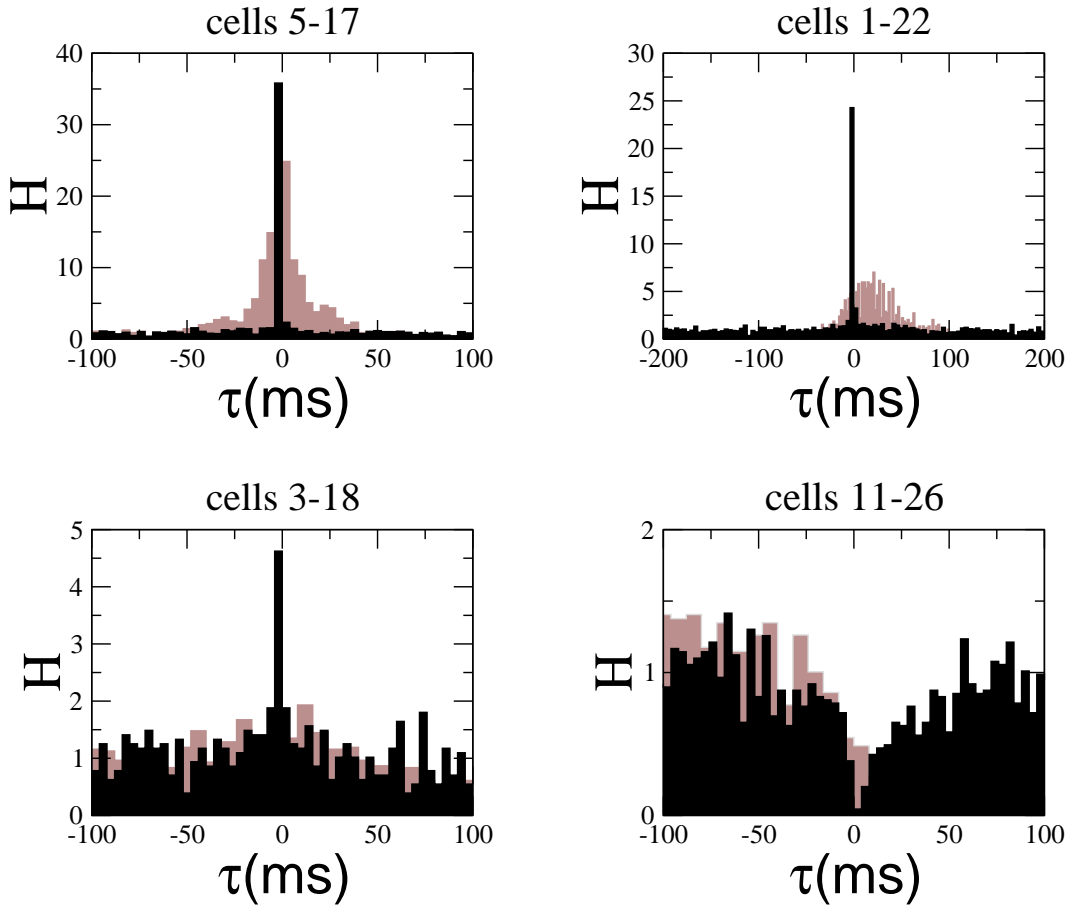


FIG. 15: Cross-correlograms H for four pairs of cells obtained from: (black histogram) the simulation of the I&F model for 32 cells with the inferred couplings and currents obtained from Dark data set and (grey histogram) directly from the experiment. Parameters for the inference and simulations are: refractory period $t_r = 5$ ms, inverse membrane leaking time $g = 0$, and noise variance $\sigma = 1$.

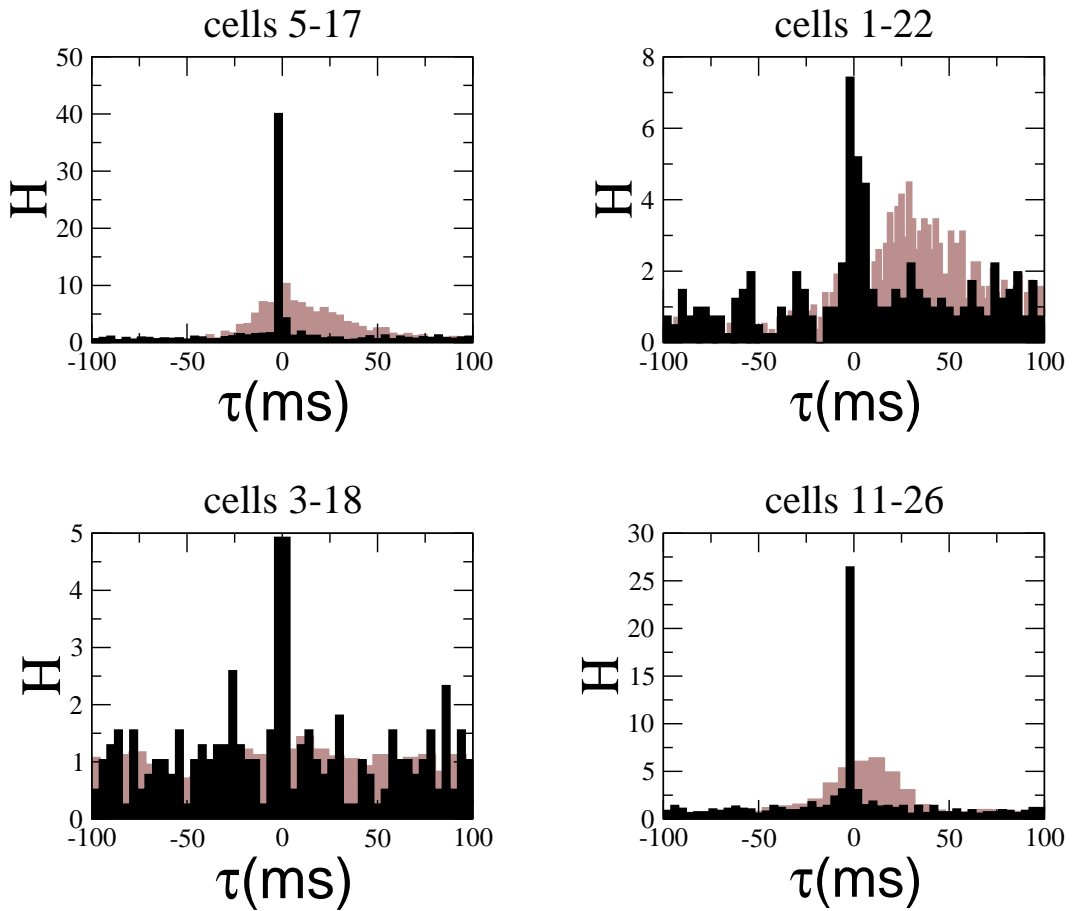


FIG. 16: Same as Figure 15 for Flicker.

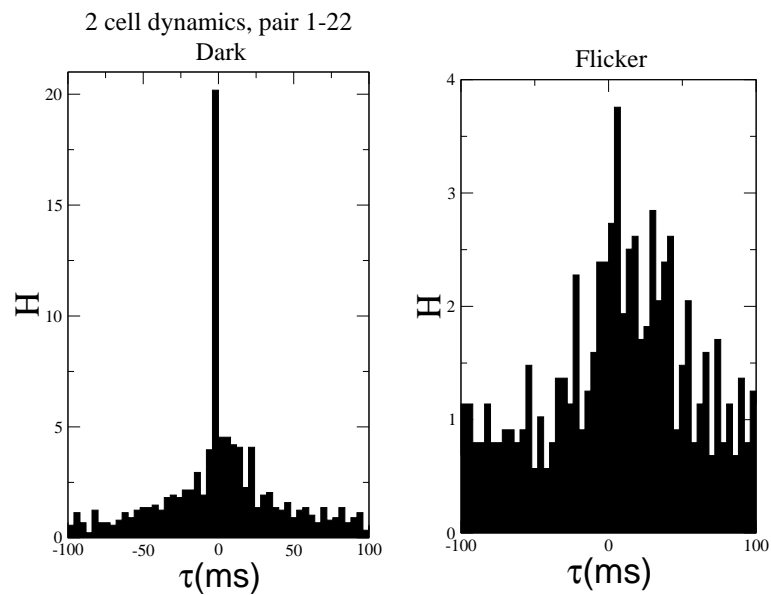


FIG. 17: Cross-correlograms for pair 1-22 obtained from the simulation of the I&F dynamics of the two cells with couplings and currents inferred from the analysis of Dark (left) and Flicker (right) data set. Same parameters as in Figure 15.

Supporting Information Appendix, Section 5:

Correspondence between Integrate-and-Fire and Ising Inverse Models

The Ising and Integrate-and-Fire (I&F) models are *a priori* very different in their assumptions and definitions. Nevertheless, there is a strong interrelation between the values of the couplings found with these two models as shown in Figure 3 of the main paper and Figure 18 below. This figure shows that positive Ising couplings, J_{ij} , and symmetrized Integrate-and-Fire (I&F) couplings, $\frac{1}{2}(G_{ij} + G_{ji})$, are very similar up to a multiplicative factor close to 0.6 in Dark and in Flicker. This is also the case for structured stimulus, called Natural Movie (Supporting Information 1, Section IV). For negative couplings, the slope is smaller and the dispersion around the linear fit is larger, especially for Flicker and Natural Movie stimuli.

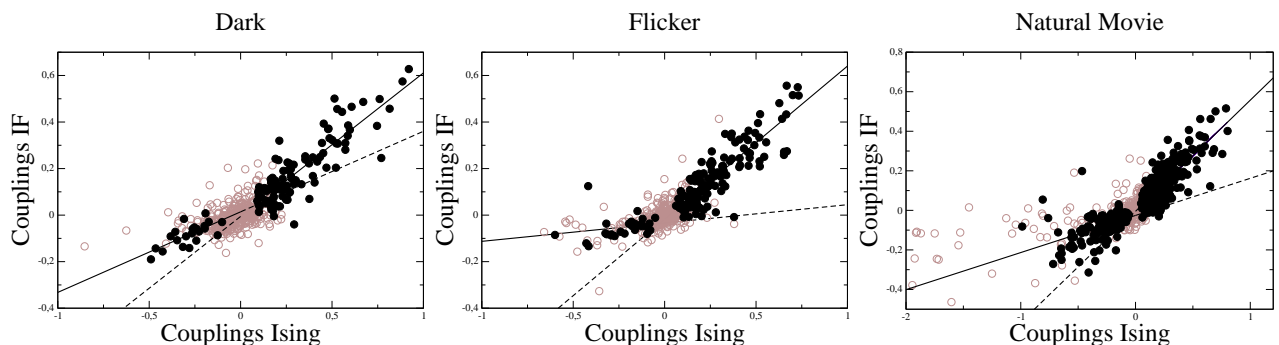


FIG. 18: Ising couplings J_{ij} vs. Integrate-and-Fire symmetrized interactions $(G_{ij} + G_{ji})/2$ for Dark (left), Flicker (middle) and Natural Movie (right) stimuli. The leak conductance g is assumed to be zero; results are unchanged as long as $1/g$ is larger than the average inter-spike interval (from 100 ms to 10s depending on the neuron). I&F couplings are expressed in the units of threshold potential V_{th} . Lines show linear fits of reliable positive couplings and reliable negative couplings. The slopes of the fits are 0.62 for positive and 0.35 for negative couplings in Dark (left); 0.66 for positive and 0.07 for negative couplings in Flicker (middle), and 0.56 for positive and 0.18 for negative couplings in Natural Movie (bottom). Notice how the dispersion of negative couplings around the linear fit line increases as one goes from Dark to Natural Movie, see text. Flicker and Dark figures are the same ones as in Figure 3 of the main paper, except that we have extended the range of linear fit. In particular, the fit calculated from negative reliable couplings in Dark seems to extrapolate to a few pairs of cells with positive couplings (large in Ising and small in I&F). These pairs of cells have unusual cross-correlograms compared to typical pairs with positive couplings e.g. pair 5-17, see below.

We now present a simple argument to explain this simple piece-wise linear relationship. For this, we consider a set of two interacting cells. We use approximate expressions for the I&F couplings (Section I) and establish a connection between the approximate expressions of the Ising and I&F couplings through the cross-correlograms of emitted spikes (Section II). Finally, we study the difference between the couplings G_{ij} and G_{ji} for a given pair of cells i, j in the I&F model (Section III).

I. APPROXIMATE EXPRESSION FOR THE I&F COUPLING

A. Calculation of the I&F coupling

Let N_1 and N_2 be the number of spikes emitted by the cells 1 and 2, and $t_{1,a}$ with $a = 1, \dots, N_1$ and $t_{2,b}$ with $b = 1, \dots, N_2$ be the times of spiking. $f_1 = N_1/T$, $f_2 = N_2/T$, where T is the duration of the recording, are the average spiking rates of the cells.

We are going to infer the coupling G_{IF} from cell 2 to cell 1 within a non-leaky I&F model (with infinite membrane decay time, i.e. in practice larger than the typical inter-spike intervals). Another quantity of interest is the external current I incoming onto cell 1.

Consider the potential $V_1(t)$ of the first cell. The threshold potential is V_{th} . Right after the a^{th} spike of the cell 1 we have $V_1(t_{1,a}^+) = 0$ while $V_1(t_{1,a+1}^+) = 1$. We consider the limit of small noise variance σ^2 and we look for the optimal path for the potential satisfying those two boundary conditions and increasing by G_{IF} each time the second cell emits a spike. For the sake of simplicity we relax the constraint that V_1 never crosses the threshold potential V_{th} at intermediate times; this approximation makes the problem much simpler but is justified only for small couplings. The log-likelihood of the optimal path for the potential is

$$\mathcal{L} = -\frac{1}{2\sigma^2} \sum_{a=1}^{N_1-1} \frac{(V_s - G_{IF} n_a - I \Delta_a)^2}{\Delta_a} \quad (40)$$

where n_a is the number of spikes emitted by the cell 2 in the a^{th} inter-spike interval of the cell 1, and $\Delta_a = t_{1,a+1} - t_{1,a}$. \mathcal{L} is a quadratic function of the current I and the coupling G_{IF} . Its maximum is reached when the coupling is equal to

$$\frac{G_{IF}}{V_{th}} = \frac{Q_1 T - (N_1 - 1) N_2}{Q_2 T - N_2^2} \quad (41)$$

where

$$Q_1 = \sum_{a=1}^{N_1-1} \frac{n_a}{\Delta_a}$$

$$Q_2 = \sum_{a=1}^{N_1-1} \frac{(n_a)^2}{\Delta_a}. \quad (42)$$

From now on we set V_{th} to unity, which means that couplings are measured in units of V_{th} .

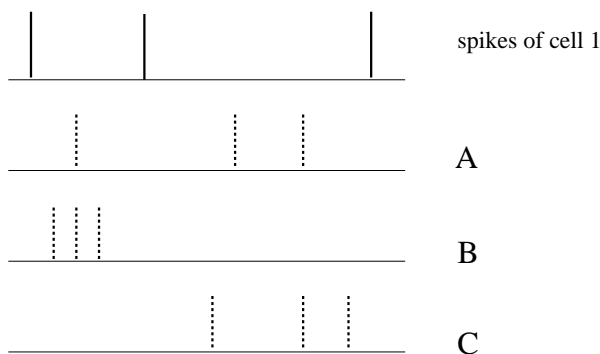


FIG. 19: A simple example of recording where both the first and the second cell emit 3 spikes each. A: the second cell emits two spikes in the second inter-spike interval of the first cell, and one spike in the first interval. B: the second cell emits all three spikes in the first interval. C: the second cell emits all three spikes in the second interval.

B. Illustration by a simple example

A simple example helps to understand the meaning of formula (43). Assume that the first cell emits $N_1 = 3$ spikes with inter-spike intervals $\Delta_1 = 1$, $\Delta_2 = 2 \times \Delta_1$, see Figure 19; the total duration is $T = 3$. The number of spikes emitted by the second cell is $N_2 = 3$. Three cases are possible:

- Case A: When the instantaneous rate of the second cell in each inter-spike interval of the first cell is equal to the average rate, we obtain $Q_1 = 2$ from (42) and the coupling $G_{IF} = 0$.
- case B: When all three spikes are emitted in the first (shorter) inter-spike interval, we obtain $Q_1 = 3, Q_2 = 9$ and $G_{IF} = \frac{1}{6} > 0$.
- case C: When all three spikes are emitted in the second (longer) inter-spike interval, we obtain $Q_1 = \frac{3}{2}, Q_2 = \frac{9}{2}$ and $G_{IF} = -\frac{1}{3} < 0$.

The interpretation of the coupling signs is rather straightforward. In case B, for instance, comparing the first and the second inter-spike intervals of the first cell, we observe that the presence of the spikes emitted from the second cell effectively shortens the inter-spike interval duration, hence the coupling is expected to be positive. In case C, on the other hand, the spikes from the second cell effectively render the second inter-spike intervals longer and thus the coupling is negative.

C. The case of Poisson statistics

We now approximate Q_2 with its value for independent cells with Poisson spiking statistics. This additional approximation is justified for small couplings since it amounts to neglecting $O(G_{IF})$ terms in the denominator of (41), and thus does not affect the leading order contribution to G_{IF} . The number of spikes n_a fired by the second cell during the time interval Δ_a (when uncorrelated with the first cell) obeys a Poisson distribution with parameter $f_2 \Delta_a$. Its second moment is $(f_2 \Delta_a)^2 + f_2 \Delta_a$, from which we deduce $Q_2 = N_1 \times (f_2 + (f_2)^2 / f_1)$ (Note that, in general, $N_1 \gg 1$ and $O(1/N_1)$ terms can be neglected). Finally, we end up with the simpler expression for the coupling

$$\frac{G_{IF}}{V_{th}} = \frac{Q_1}{N_1 f_2} - 1 . \quad (43)$$

II. RELATIONSHIP WITH THE CROSS-CORRELOGRAMS

We recall that the definitions of cross-correlograms and of the correlation index are given in Supporting Information 4.

A. From the correlation index to the Ising coupling

Our approximation for the Ising coupling is identical to the lowest order approximation described in Supporting Informations 1&4. Let Δt denote the time-bin width. We call p_1 (or p_2) the probabilities that cell 1 (or 2) emits one, or more spikes in a time-interval bin, and p_{12} the probability that they are both active. To the lowest order of our diagrammatic expansion, the Ising coupling between the two cells can be expressed as:

$$J_{Ising} = \frac{1}{4} \left(\frac{p_{12}}{p_1 p_2} - 1 \right) . \quad (44)$$

from Eqs. (34) and (35). We check that Δt is much smaller than the typical inter-spike interval durations of the two cells (in Flicker and Dark the firing rates range from 0.1 to 2 Hz, while Δt is of the order of 10 ms). Then multiple spikes of the same cell in a bin are very unlikely.

B. From the correlation index to the I&F coupling

To calculate Q_1 , we need to know how many spikes of the second cell enter the first one in an inter-spike interval. Let us assume that all the inter-spike intervals of the first cell have equal durations $1/f_1$. Then the delay between

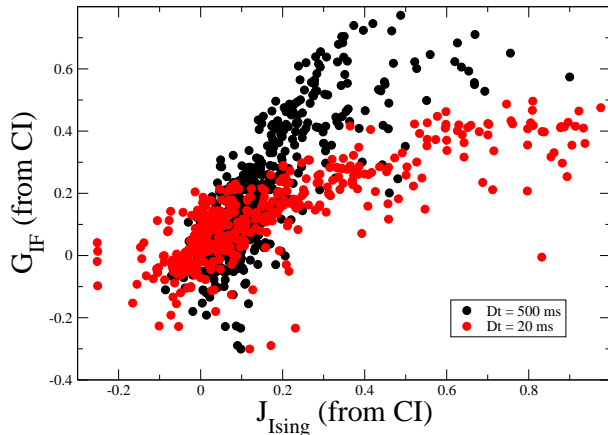


FIG. 20: I&F vs. Ising couplings from the CI approximation (45) for two values of Δt .

a spike of the second cell and spikes of the first cell, defining the boundaries of the inter-spike interval, is equal at most to $1/(2f_1)$, and Q_1 coincides with the correlation index on this time scale, $Q_1 \simeq N_1 f_2 CI(1/f_1)$. Due to the variability of the durations of the inter-spike intervals of the first cell this estimate for Q_1 is not exact: we should average CI over those durations rather than calculating the correlation index for the average duration.

C. Conclusion

We end up, therefore, with the following approximate expressions for the couplings

$$J_{Ising} \simeq \frac{1}{4}(CI(\Delta t) - 1)$$

$$G_{IF}(2 \rightarrow 1) \simeq CI(1/f_1) - 1 \quad , \quad G_{IF}(1 \rightarrow 2) \simeq CI(1/f_2) - 1 . \quad (45)$$

No obvious relationship exists between the I&F couplings from the first to the second cell and from the second to the first cell, except when the rates f_1 and f_2 are close to one another.

As evoked above, the typical inter-spike interval is of duration 1 sec in Flicker or Dark, while Δt is much shorter. Hence, for cross-correlograms with a positive peak (Flicker in Figure 2 of the main text) J_{Ising} will be larger than G_{IF} . On the other hand, for cross-correlograms with a negative dip (Dark in Figure 2 of the main text) J_{Ising} will be lower than G_{IF} . These statements qualitatively reproduce what was observed in Figure 18.

We also see that the 0.6 slope observed in Figure 18 is an average property. The ratio G_{IF}/J_{Ising} depends on the firing rates of each cell. However, most of positive couplings correspond to cross-correlograms with a strong positive peak, centered in zero, as in Figure 2 of the main text (Flicker). For the latter cross-correlogram, we estimate $J_{Ising} \simeq 1.5$ and $G_{IF} \simeq 0.6$ from (45). Hence, the ratio between the two couplings of this particular pair is equal to 0.4.

As Δt varies the CI changes, as shown in Figure 14 in Supporting Information 4, and so does the Ising coupling. For large Δt the Ising couplings are expected to be similar to their I&F counterparts as shown in Figure 20.

Some negative Ising couplings J_{ij} correspond to cross-correlograms H_{ij} with a shifted positive peak, *i.e.* with a delay larger than Δt . Contrary to the Ising model the I&F model is able to capture such delayed and positive correlations, with the result that G_{ij} is positive. Hence, we expect a strong discrepancy between Ising and I&F couplings for those pairs of cells. This can indeed be seen on Figure 18, where the dispersion around the linear fit for negative couplings is weak for Dark, for which few delayed cross-correlograms are found, and gets larger for structured stimuli such as Flicker and, above all, Natural Movie.

III. ON THE SYMMETRY OF COUPLINGS IN THE I&F MODEL

The above sections have shown a piece-wise linear relationship between the Ising couplings and the symmetrized I&F couplings, $\frac{1}{2}(G_{ij} + G_{ji})$. Hereafter we study how symmetric are the couplings in the I&F model.

In Figure 21 we compare the couplings G_{ij} and G_{ji} extracted from the Integrate-and-Fire model for every pair i, j of cells. While G_{ij} strongly differs from G_{ji} for some pairs of cells especially in Dark, there is a clear interrelation (positive correlation) between G_{ij} and G_{ji} for most pairs of cells.

It is tempting to interpret the above results from a physiological point of view. Couplings in the third quadrant, *i.e.* such that both G_{ij} and G_{ji} are negative are compatible with lateral inhibition effects. The quasi-absence of pairs (i, j) such that G_{ij} and G_{ji} have opposite signs suggest that some pathways from the photo-receptors to the ganglion cells may inhibit another pathways to different ganglion cells, but that the inhibition is not reciprocal.

Let us stress that Fig. 21 has been obtained in the limit of a vanishing leak-conductance g . It would interesting to study how the pattern of symmetry changes with the value of g .

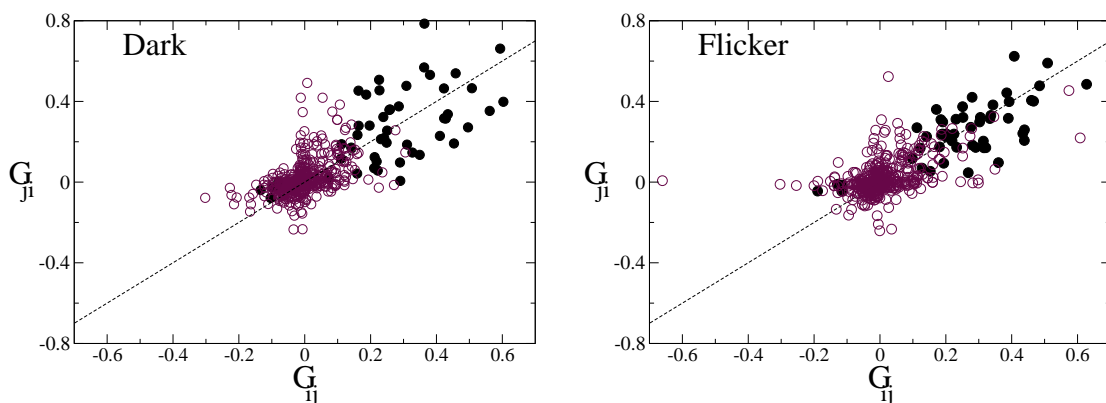


FIG. 21: Integrate-and-Fire model effective couplings G_{ij} versus G_{ji} : Full circles represent the top 10% of reliable couplings, *i.e.* the couplings with the smallest relative errors, empty circles represent the remaining couplings. The dashed line has slope unity.

Supporting Information Appendix, Section 6:

Spatial features of the inferred couplings

Here we deal with two related questions:

- how do the coupling J_{ij} vary with the distance between the (receptive fields of the) cells i and j ? As a complement to Figure 5 in the main text, we show here the map of smallest Ising couplings and the map of largest correlations in the retinal plane. This issue is discussed in Section I below.
- how much does the inferred value for the coupling J_{ij} depend on the activity of other cells located at some distance of cells i and j ? This last question is of fundamental importance since most cells are not recorded in the experiments, and it is legitimate to wonder whether the couplings inferred from only a small portion of the retina are meaningful. To answer this question we use linear response theory (Section II), which allows us to quantify changes in the couplings when some cells are removed from the recordings. Conclusions are presented in Section III.

I. DEPENDENCE OF THE COUPLINGS ON THE DISTANCE BETWEEN CELLS

Figure 5 in the main paper shows the network of interactions in the retina obtained from Ising and I&F strong couplings, for Dark (40 links) and Flicker (48 links) stimuli. In Figure 22 we plot the network of interactions between cells obtained from the smallest (including negative) reliable couplings in Dark and Flicker. We keep the number of couplings the same as in Figure 5 of the main paper in order to allow for a comparison. The 'nearest-neighbour' nature of the interaction network, obtained from the large couplings in Dark and from the large couplings conserved in Flicker and Dark is not reproduced with small couplings. In Flicker long-range couplings are much more frequent than in the Figure 5 of the main paper. This comparison supports the idea that the network of interactions defined from the set of strong positive couplings is very far from being random.

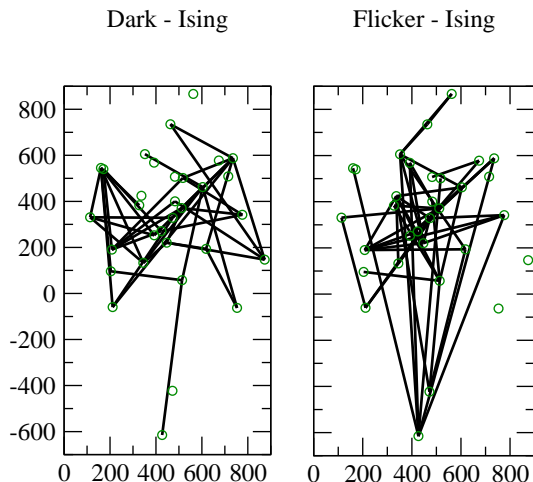


FIG. 22: Maps of the smallest reliable couplings (top) in the retinal plane for Dark (left) and Flicker (right) stimuli. The circles represent the centers of the receptive fields of the 32 cells. Each edge correspond to one of the smallest M reliable couplings J_{ij} (top) or largest M connected correlations c_{ij} (bottom), with $M = 40$ in Dark and $M = 47$ in Flicker. The numbers of links are chosen to be the same as in Figure 5 of the main text to facilitate the visual comparison with this figure.

Figure 23 (top) shows the graphs obtained from the largest correlations c_{ij} instead of the couplings J_{ij} (with the same numbers of links). The structure of the coupling and correlation networks are not identical; in particular some cells are much more connected (have higher 'degree of connectivity') in the correlation network than in the coupling network. The map of the largest correlation indices, or, equivalently, the largest 2-cell couplings J_{ij}^{2-cell} , shown in Fig. 23 (bottom) is in a better agreement with Figure 5 of the main text. Indeed, as discussed in Supporting Information 4, the large and positive J_{ij}^{2-cell} are a good approximation to large and positive couplings in the two analyzed data sets.

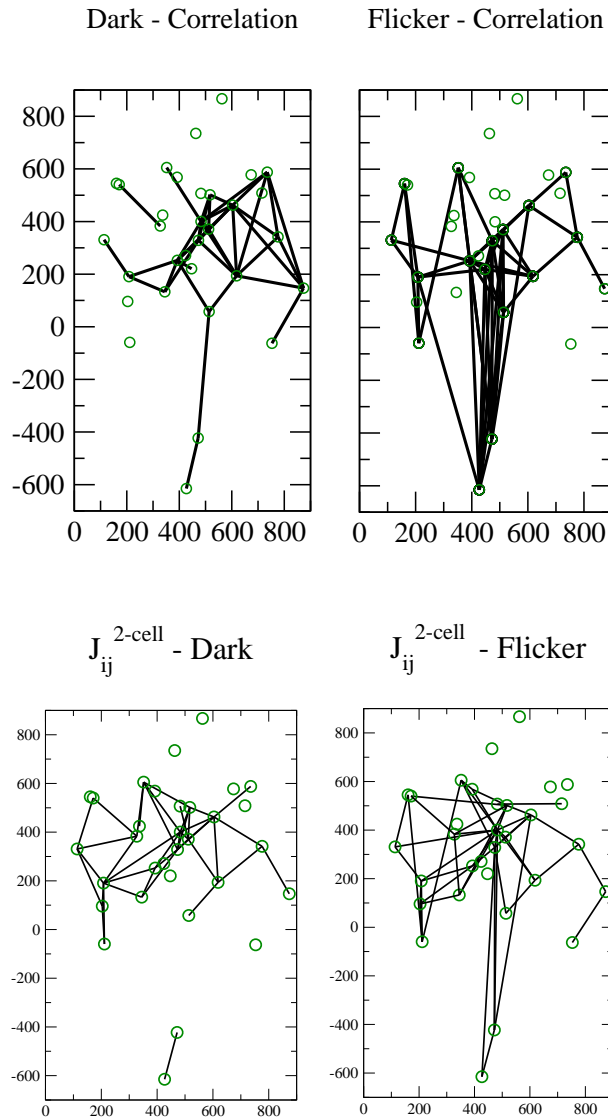


FIG. 23: Maps of largest connected correlations (top) and largest correlation index in the retinal plane for Dark (left) and Flicker (right) stimuli. The circles represent the centers of the receptive fields of the 32 cells. The numbers of links are chosen to be the same as in Figure 5 of the main text to facilitate the visual comparison with this figure. Top: Each edge correspond to one of the largest M connected correlations c_{ij} (top), with $M = 40$ in Dark and $M = 48$ in Flicker. Bottom: Each edge represents one of largest M correlation indices with $M = 40$ in Dark *i.e.* $J_{ij}^{2-cell} = \log CI_{ij}/4 > 0.26$, and $M = 48$ in Flicker *i.e.* $J_{ij}^{2-cell} = \log CI_{ij}/4 > 0.23$.

II. CALCULATION OF THE LINEAR RESPONSE TO THE REMOVAL OF A COUPLING OR A FIELD

We aim to calculate the change in the inferred coupling or field values when some cells are removed from the pool of measured neurons. We first calculate the couplings for a large set of $M + n$ cells, then remove M cells and want to calculate the changes in the couplings $\{J_{ij}\}$ between the n cells (Figure 24). By removing the cells we mean ignoring them or, to be precise, not imposing the pair-wise correlations between those cells. The constraints enforcing that the spin-spin correlations in the Ising model are equal to their experimental values are released by setting all the couplings $\{J_{kl}\}$ inside a subset M and the couplings $\{J_{ik}\}$ between subsets M and n to zero.

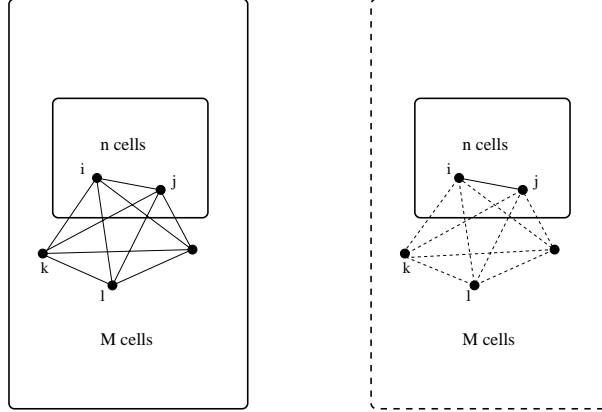


FIG. 24: Set of $M + n$ neurons (left) from which M neurons are removed (right). The constraints on the pair-wise correlations between two removed cells, or one removed cell and one remaining cell are released by setting the corresponding couplings to zero, see text.

When turning off those couplings the firing probability $\{p_i\}$ and correlations $\{c_{ij}\}$ inside the remaining set of n cells would change if the fields $\{h_i\}$ and couplings $\{J_{ij}\}$ were left unaltered. Of course, the constraints on the correlations between the remaining cells are not released, hence the corresponding values of fields and couplings will change by $\{\Delta h_i\}$ and $\{\Delta J_{ij}\}$, respectively. The average activities and correlations of the subset of n cells after turning off the outside couplings, $\{\tilde{p}_i\}$, $\{\tilde{c}_{ij}\}$, are calculated from the values inferred before turning off the couplings, $\{p_i\}$, $\{c_{ij}\}$. Within the framework of linear response theory:

$$\begin{aligned}\tilde{p}_i &= \frac{1}{2} \frac{\partial \ln Z}{\partial h_i} [\{h_i + \Delta h_i\}, \{J_{ij} + \Delta J_{ij}\}, \{h_k\}, \{J_{kl} + \Delta J_{kl}\}, \{J_{ik} + \Delta J_{ik}\}] \\ \tilde{c}_{ij} &= \frac{1}{4} \frac{\partial \ln Z}{\partial J_{ij}} [\{h_i + \Delta h_i\}, \{J_{ij} + \Delta J_{ij}\}, \{h_k\}, \{J_{kl} + \Delta J_{kl}\}, \{J_{ik} + \Delta J_{ik}\}] .\end{aligned}\quad (46)$$

Expanding to first order in the fields and couplings around their values before the removal of cells with changes $\Delta J_{kl} = -J_{kl}$, $\Delta J_{ik} = -J_{ik}$ and imposing that the average activities and correlations have not changed, $\{\tilde{p}_i = p_i\}$, $\{\tilde{c}_{ij} = c_{ij}\}$, we obtain:

$$\sum_{a'=\{i',\{i',j'\}\}} H_{a,a'} \Delta v_{a'} = \sum_{b'=\{i',k'\},\{k'',l'\}} H_{a,b'} J_{b'} \quad (47)$$

where $\vec{\Delta v} = (\Delta h_1, \dots, \Delta h_n, \Delta J_{12} \dots \Delta J_{n-1,n})$ is the vector of fields and couplings variations in the remaining subset of cells with $n \times (n-1)/2$ components; $\vec{J} = (J_{1,n+1}, \dots, J_{n,M}, J_{n+1,n+2}, \dots, J_{M-1,M})$ is the vector of removed couplings; and the susceptibility matrix is

$$\mathbf{H} = \begin{pmatrix} \frac{\partial^2 \ln Z}{\partial h_i \partial h_{i'}} & \frac{\partial^2 \ln Z}{\partial h_i \partial J_{k'l'}} \\ \frac{\partial^2 \ln Z}{\partial h_{i'} \partial J_{kl}} & \frac{\partial^2 \ln Z}{\partial J_{kl} \partial J_{k'l'}} \end{pmatrix} = \begin{pmatrix} 4 (\langle s_i s_{i'} \rangle - \langle s_i \rangle \langle s_{i'} \rangle) & 8 (\langle s_i s_{k'} s_{l'} \rangle - \langle s_i \rangle \langle s_{k'} s_{l'} \rangle) \\ 8 (\langle s_{i'} s_k s_l \rangle - \langle s_{i'} \rangle \langle s_k s_l \rangle) & 16 (\langle s_k s_l s_{k'} s_{l'} \rangle - \langle s_k s_l \rangle \langle s_{k'} s_{l'} \rangle) \end{pmatrix}, \quad (48)$$

where $\langle \cdot \rangle$ denotes the average with Gibbs measure given by the Ising model, and $i = 1, \dots, N$, $1 \leq k < l \leq N$. Calling $\hat{\mathbf{H}}$ the restriction of the matrix \mathbf{H} to the subset of n cells we obtain

$$\Delta v_a = \sum_{a'=\{i'\},\{i',j'\}} \sum_{b'=\{i',k'\},\{k'',l'\}} (\hat{H}_{a,a'})^{-1} H_{a,b'} J_{b'} \quad (49)$$

In practice, we calculate the susceptibility matrix \mathbf{H} from the 4-spin correlations in the data, rather than through the Monte-Carlo simulations. We have checked that the choice of this method, which requires much less computation time, does not affect the results.

A. Applications

In this section, we call $D(i, j)$ the distance between the centers of the receptive fields of cells i and j in the plane of the retina. The largest distance in the analyzed data sets is equal to about 1.5 mm. All results are presented for a binning time $\Delta t = 20$ ms, except Figures 27 and 28 for which $\Delta t = 10$ ms.

1. Removal of a single cell

We now apply the linear response theory to study how the couplings change when one cell is removed from the set of registered neurons. More precisely, we turn off the couplings between 31 cells and the cell number k , and then calculate the change ΔJ_{ij} of the interactions between the $31 \times 30/2 = 465$ pairs of remaining cells. Each change ΔJ_{ij} is plotted versus the distance between the pair i, j and the cell k defined as

$$d(i, j; k) = \frac{1}{2} [D(i, k) + D(j, k)] . \quad (50)$$

Results are shown in Figure 25 for two examples of the choice of the removed cell, the cells 2 and 13. The cell 2 seems to be representative of the most of recorded cells. The observed changes in Dark are of amplitude 0.1 or less, and do not spread above distances of 500-600 μm . The amplitude in Flicker conditions is much (about 10 times) smaller. This is due to the increased number of spikes under Flicker stimuli, which makes smaller the number of pairs never firing together in the same bin. The smallest eigenvalue of the susceptibility matrix of large assemblies of cells are thus smaller in Dark than in Flicker, and are of the order of the Bayesian *a priori* parameter Γ . Hence, the response to a change is often larger in Dark than under Flicker stimuli.

Figure 25 shows that the typical response to removal of the cell 13 in Dark is 10 times smaller than for the cell 2, and even smaller than its value in Flicker conditions. The cell 13 is located on the distant part of the retinal map, far away from most other neurons. It is weakly connected to any other cell (except the cell 19, see retinal map), and removal of cell 13 basically does not affect other couplings.

2. Removal of all but two cells

We now consider another extreme case. We start from the set of 32 cells, and remove all cells but two, say, i and j . In practice, we turn off $30 \times 29/2 - 1 = 435$ couplings between the 30 removed cells, and $30 \times 2 = 60$ interactions between one of those 30 cells and one of the two remaining neurons i, j . The change in the coupling between the cells i, j is calculated as a linear superposition of all changes in the 495 couplings and plotted versus the distance between pairs i, j and k, l defined through

$$d(i, j; k, l) = \frac{1}{2} [\min(D(i, k), D(j, k)) + \min(D(i, l), D(j, l))] . \quad (51)$$

Results are shown in Figure 26 for four pairs of cells i, j . It appears that the response in Dark vanishes for distances above 600 μm , see cells 13-19 and 4-15, which are the only pairs with strong positive couplings allowing us to explore such distances. Notice also the pair 1-2, for which the response in Dark vanishes at smaller distances than in Flicker. In Flicker response at larger distances exists for some pairs (e.g. 13-19) while it is absent for other pairs (e.g. 4-15).

It is interesting to note that the pair 11-26, which corresponds to a strong positive coupling at a large distance in Flicker, and has a negative coupling in Dark, responds only very weakly to the removal of all other cells in Flicker.

The behavior of the response is correlated to the velocity of convergence of the inference algorithm (see Figure 1 in the main paper). For some pairs of cells the 2-cell approximation (all diagrams with those 2 cells only) is excellent, the convergence is fast and the susceptibility is small. For other pairs the susceptibility is larger or decreases at larger

distances and one needs to take into account larger orders in the diagrammatic expansion to obtain a good estimate of the coupling. These two behaviors may be found for the same pair when changing the stimulus, e.g. the pair 13-19 with the response smaller in Flicker than in Dark.

3. Change in the couplings with the number of cells

We see from the above Figures that the amplitude of responses is small (between .01 and .1), compared to the value of strong couplings (with value about 1). In addition, the responses may be positive or negative, with an average value close to 0.

This statement explains the apparent lack of changes in the couplings, seen in Figure 27, when shifting from 9 to 12 cells. From a similar picture with a small number of cells (about 10), Schneidman et al. [1] concluded that the couplings do not change with the number of cells, N . Figure 28 clearly shows that the couplings change values when one extends the analysis from 12 to 32 cells. That many strong couplings are relatively insensitive to N is not surprising: they are very well approximated by the 2-cell formula and do not depend on the neighboring activities. On the contrary, small or negative couplings are often network properties and are affected by the number of cells.

4. Conclusion

From the above analysis it appears that:

- Changes in Dark do not spread over distances larger than 500-600 μm .
- Long-range couplings, which are stimulus-dependent (present in Flicker, but not in Dark, e.g. the pair 11-26) may not be sensitive to removal of other cells. In other words the range of a coupling J_{ij} (distance between the cells i, j) has nothing to do with the range of the susceptibility (distance over which J_{ij} responds to removal of one cell).
- Removal of one distant cell (e.g. 13) has less consequence on the couplings than removal of a central cell (e.g. 2).
- Couplings that are accurately inferred from the 2-cell approximation are insensitive to removal of other cells (apart from the two cells in the pair). This means that they are accurately predicted even if only a small area of the retina is recorded. Negative couplings, on the other hand, are more affected by other cells (and by the number of cells, N , see Figure 28).

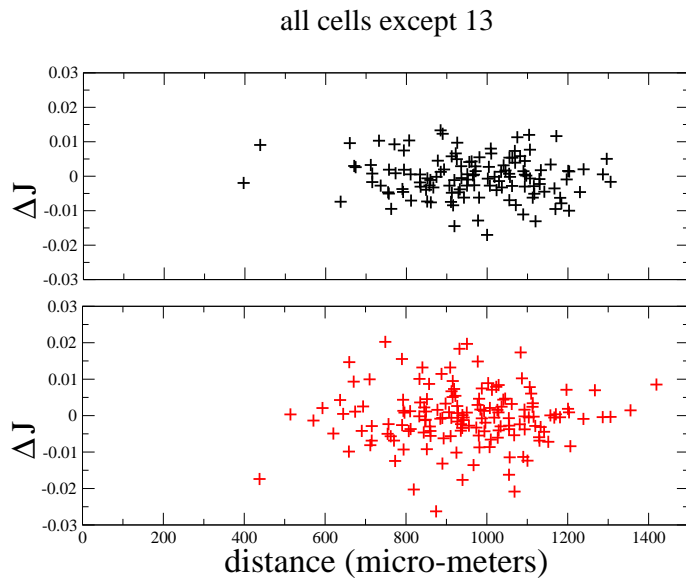
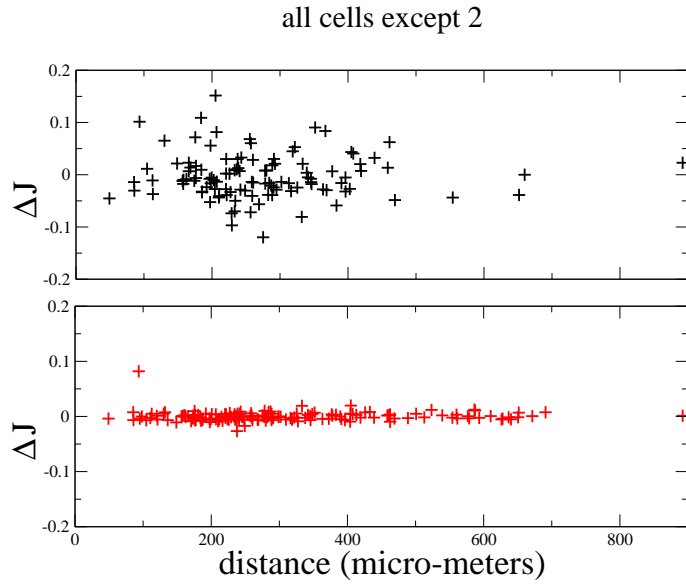


FIG. 25: Changes in the coupling J_{ij} between the cells i and j , when the cell k is removed from the pool of 32 recorded neurons, as a function of the distances between pairs i, j and cell k , Eq. (50), and for cells $k = 2$ and 13 . Only reliable pairs i, j , *i.e.* such that the relative error on the inferred couplings with the full set of 32 neurons is smaller than 30%, are shown.

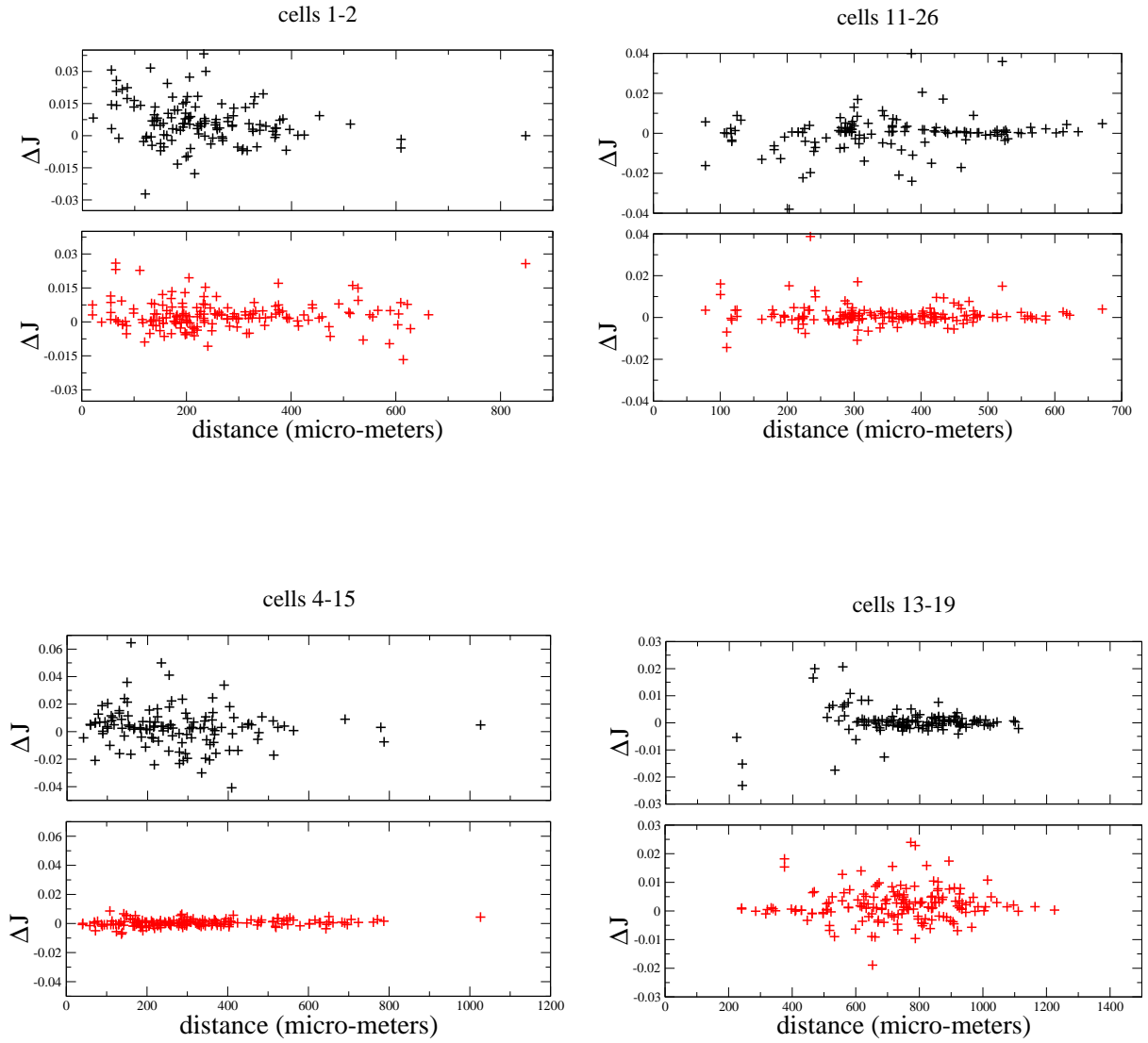


FIG. 26: Change in the coupling J_{ij} between cells i and j , when the correlations between cells k, l are no longer imposed, as a function of the distances between the pairs i, j and k, l (51), and for pairs $i, j = 1, 2; 4, 15; 11, 26; 13, 19$. Only reliable pairs k, l are shown, i.e. pairs with the relative error on the inferred couplings (with the full set of 32 neurons) smaller than 30%

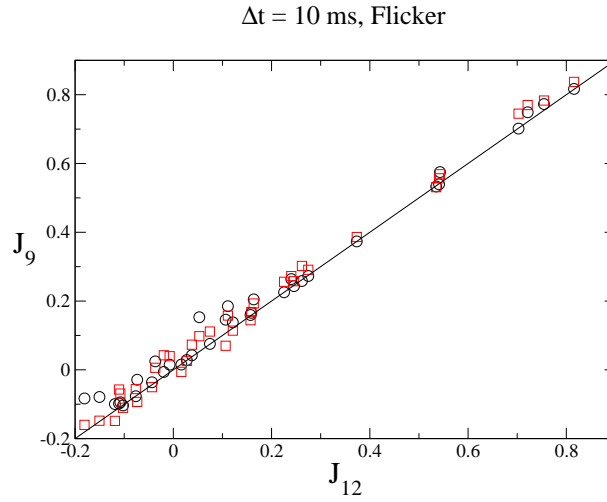


FIG. 27: Couplings J_{ij} for the 36 pairs between the first 9 cells (Flicker, $\Delta t = 10$ ms) as a function of their values, when 3 more cells are added. Black circles are deduced from an exact calculation, while red squares are results from the linear response theory after the removal of the last 3 cells from the set of 12, see Section II.

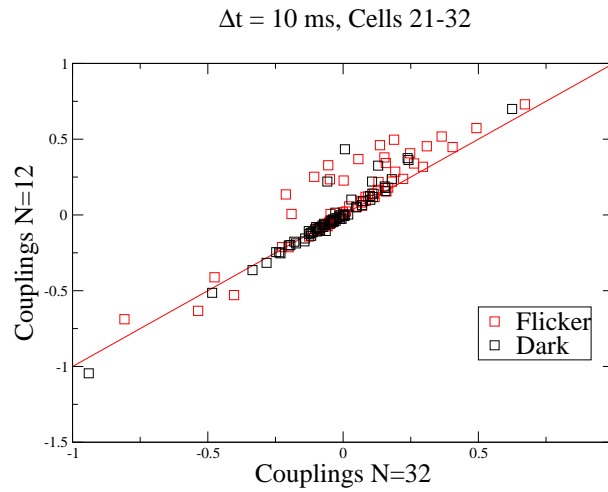


FIG. 28: Couplings J_{ij} for Flicker, $\Delta t = 10$ ms, when changing from 12 to 32 cells.

Supporting Information Appendix, Section 7:

On states and the large- N limit in the Ising model

Schneidman et al. discuss in [1] the dependence of the values of the couplings and fields with the number N of neurons in the data set. Based on the analysis of a small number of neurons ($N < 15$), they state that the average value of J does not change with N . This scaling, extrapolated to large sizes N , is unusual for Ising models, where the average coupling generally decreases with N [23]. According to Schneidman et al. the extrapolation indicates that the energy becomes much larger than the entropy or, in other words, that the effective temperature of the Ising model tends to zero as N increases. If this were true, only the configurations minimizing the energy would have a non negligible probability in the large N limit. These configurations, called frozen states, are reminiscent of spin-glass states and are claimed to play an important role in error correction in [1].

The extrapolation to large values of N , much larger than the population of the registered cells, raises several concerns. First it is not clear whether the Ising representation of the firing activity is really accurate when N grows, see Supporting Information 2. Secondly, we have found in Supporting Information-6 that the coupling between a pair of cells generally depends on the activity of nearby cells, and hence may vary with N . Thirdly, the uncertainty on the inferred couplings depend on N too, which could make the extrapolation quantitatively unreliable.

Hereafter, we show that there is no need to actually solve the inverse Ising problem to decide whether one or multiple states are present. Our approach is based on the spectral analysis of the correlation matrix (Section I) and its relationship with the existence of one or more states (Section II). We mainly focus on a recording of the activity of 40 neurons in a retina presented with a natural movie stimulus (data courtesy of M. Berry) to allow the comparison with ref [1] (Section III). Our analysis provides strong support for the existence of only one state in Natural-Movie, when the time-bin interval Δt is a few tens of ms; this result holds for Flicker and Dark stimuli as well.

I. SPECTRAL ANALYSIS OF THE CORRELATION MATRIX

For the simplicity of the presentation it is convenient to consider spins with ± 1 values; we thus define $\sigma_i = -1 + 2s_i = \pm 1$, where $s_i = 0, 1$ are the variables defined in the main text (0 if cell i is silent in a given bin, 1 if it is active). The Ising model Gibbs measure (Supporting Information-1, formula 1) over the s_i -spins induce a measure over the σ_i -spins. We use the notations $m_i = \langle \sigma_i \rangle$ for the spin magnetization, and $C_{ij} = \langle \sigma_i \sigma_j \rangle$ for the spin-spin correlation (not connected).

Let C^a , $a = 1, \dots, N$ be the eigenvalues of the correlation matrix C_{ij} , and $\{v_i^a; i = 1, 2, \dots, N\}$ the components of the corresponding eigenvectors. The normalization is chosen in the way to ensure $\sum_i (v_i^a)^2 = 1$. Figure 29 shows the largest three eigenvalues as a function of the number N of cells considered in the Natural Movie data set (qualitatively similar plots are obtained for Dark and Flicker). For small time-bin widths $\Delta t = 2$ ms, the largest eigenvalue scales linearly with N , while all smaller eigenvalues tend to finite limits as N grows. On the contrary, for very large time-bin widths, *e.g.* $\Delta t = 2$ s, all three top eigenvalues are proportional to N . As C_{ij} is bounded (by 1 in absolute value) the eigenvalues C^a proportional to N are associated to eigenvectors spreading over a finite fraction of the sites: $v_i^a = O(1/\sqrt{N})$. Such eigenvectors are called extended [15].

II. RELATIONSHIP WITH THE EXISTENCE OF STATES

How can we extract information about states from the above spectral analysis? The key point is that, when a single eigenvalue of the correlation matrix is extensive in N , there can be only one state. We briefly explain below this statement; see [14] for a detailed analysis.

An important quantity in statistical physics is the response R_{ij} of the spin i to a perturbation in j , defined as follows. Assume the field on spin j changes by a small amount, $h_j \rightarrow h_j + \delta h_j$. This perturbation will, in turn, produce a small change in the magnetization of spin i , $m_i \rightarrow m_i + \delta m_i$. Then, the response R_{ij} is the value of the ratio $\delta m_i / \delta h_j$ for an infinitesimal perturbation. The thermodynamical stability of a state requires that the response R_{ij} , for a fixed j , can be strong (finite) over a vanishingly small fraction of the spins i only. Informally speaking, a local perturbation cannot spread over the whole system.

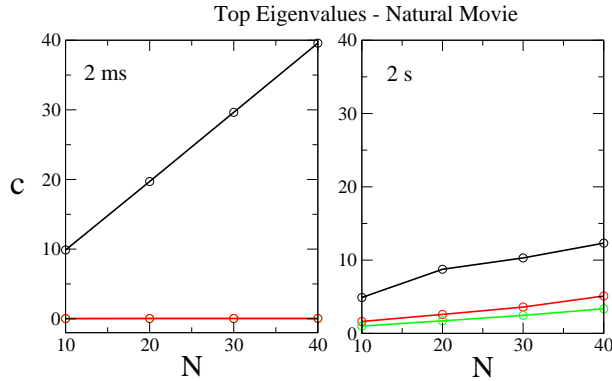


FIG. 29: Largest three eigenvalues of the correlation matrix for the Natural Movie stimulus and for $\Delta t = 2$ ms (left) and $\Delta t = 2$ s (right) as a function of the number N of cells included in the data set. The largest, second largest and third largest eigenstate are shown, in order, in black, red, and green colors. In the left panel, the second and third eigenvalues are hardly distinguishable.

The fluctuation-dissipation theorem tells us that the response coincides with the connected correlation,

$$R_{ij} = C_{ij} - m_i m_j = \sum_a C^a v_i^a v_j^a - m_i m_j . \quad (52)$$

Let us fix the location of the perturbation (site j). From Eq. (52) we can see that the perturbation will be transmitted by all the eigenmodes having both sites i and j in their support, *i.e.* having non zero components in i and j . Many eigenvectors have a finite size (not increasing with N) support, and induce a localized response to the local perturbation in j (Figure 30).

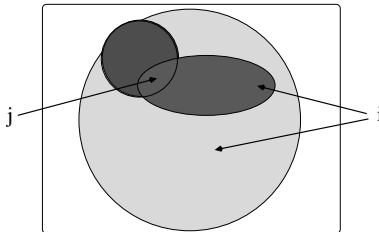


FIG. 30: The square box symbolizes the whole set of spins. The perturbed spin j belongs to the supports of some eigenvectors of the correlation matrix (three of them are sketched). A non extensive number of spins i , belonging to the supports of one of the localized eigenvectors (dark hatches), will strongly respond to the perturbation. Extended eigenvector (light hatches), which spread over a fraction of all spins, trigger a global response of the system.

We now consider the response triggered by extended eigenmodes. As extended eigenmodes have $O(1/\sqrt{N})$ components their contribution to R_{ij} is small unless the associated eigenvalues are large. Let $K(\leq N)$ be the number of extensive eigenvalues C^a . The contribution of extended eigenmodes to the response reads

$$R_{ij}^{ext} \simeq \sum_{a \leq K} C^a v_i^a v_j^a - m_i m_j , \quad (53)$$

where we have $C^a = O(N)$, $v_i^a = O(1/\sqrt{N})$ for all i and for all $a \leq K$. It is clear from (53) that R_{ij}^{ext} is non zero for almost all pairs i, j unless

$$K = 1 \quad \text{and} \quad m_i \simeq \sqrt{C^1} v_i^1 . \quad (54)$$

We deduce that, in the presence of a single state, there is only one extensive eigenvalue.

What happens if there is more than one state? The situation is reminiscent of the phase coexistence in first order phase transitions where different physical, e.g. liquid and gaseous states coexist [17]. Let us call w^α the thermodynamical weight of state α , that is, the exponential of minus its free energy. Each state, or phase, is thermodynamically stable. Hence C_{ij}^α , the spin-spin correlation matrix for state α , has a single extensive eigenvalue and the associated eigenvector fulfills (54) where the magnetization is now m_i^α , the average value of spin i in state α . Unfortunately, the data do not give access to each state correlation matrix but only to their weighted sum,

$$C_{ij} = \sum_{\alpha} w^{\alpha} C_{ij}^{\alpha} . \quad (55)$$

The weighted correlation matrix C has more than one extensive eigenvalues. To be more precise, the number K of extensive eigenvalues of C is simply the dimension of the space spanned by the magnetization vectors $\vec{m}^\alpha = (m_1^\alpha, m_2^\alpha, \dots, m_N^\alpha)$, and is larger or equal to 2. These magnetization vectors would be in one-to-one correspondence with the frozen states in Schneidman et al.'s paper.

III. ANALYSIS OF EXPERIMENTAL DATA

We now turn to the analysis of the experimental recordings. The overlap between spin configurations is defined as

$$q \equiv \frac{1}{N} \sum_{i=1}^N m_i^2 . \quad (56)$$

In the presence of a single state this overlap coincides, from (54), with

$$q = \frac{C^1}{N} . \quad (57)$$

Identity (57) can be checked from the experimental data without solving the inverse problem. We need only to calculate the local magnetizations, diagonalize C , and compare the overlap q to the largest eigenvalue C^1 of C . The outcome is shown in Figure 31. For small Δt (up to 10 ms for Natural Movies data and 100 ms for Dark data) the agreement between the overlap and the largest eigenvalue is excellent, and a single state is expected and no freezing into multiple states occurs [24]. A departure from (57) is clearly visible for large Δt , e.g. for $\Delta t > .5$ s, which may signal the existence of more than one state. However, for large values of Δt the Ising encoding of the spiking activity is questionable. No distinction is made between the firing of one or more spikes in the same time-bin, the latter causing a loss of information when Δt is larger than the typical inter-spike interval $\simeq .7$ s in Natural-Movie.

Our analysis of the spectral properties of the correlation matrix does not allow us to decide whether the freezing mechanism suggested by Schneidman et al. takes place or not. However, it contradicts the existence of multiple quasi ground-states lying far away from each other, and the spin-glass picture put forward by these authors [1].

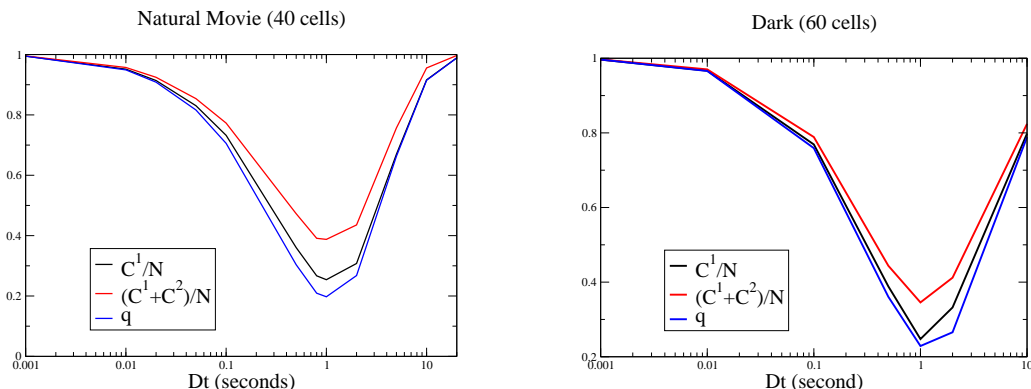


FIG. 31: Overlap q (sum of squared magnetizations (57, blue line) compared to the largest eigenvalue, and the sum of the largest two eigenvalues, of the correlation matrix as a function of Δt for Natural Movie (left) and Dark (right, all 60 cells) data. The sum of the two largest eigenvalues, divided by N , is a lower bound to the Edwards-Anderson overlap used in spin-glass literature [14, 16].

Bibliography and footnotes:

- [1] E. Schneidman, J.J. Berry II, R. Segev, W. Bialek. Weak pairwise correlations imply strongly correlated network states in a neural population. *Nature* **440**, 1007-1012 (2006).
- [2] C.S. Wallace, *Statistical and Inductive Inference by Minimum Message Length*, (Springer-Verlag, Information Science and Statistics, 2005).
- [3] T. Plefka. Convergence condition of the TAP equation for the infinite-ranged spin glass model. *J. Phys. A* **15**, 1971 (1982).
- [4] A. Georges, J. Yedidia. How to expand around mean-field theory using high-temperature expansions. *J. Phys. A* **24**, 2173 (1991).
- [5] D. McKay, *Information Theory, Inference, and Learning Algorithms*, (Cambridge University Press, 2003).
- [6] M. Schnitzer, M. Meister. Multineuronal Firing Patterns in the Signal from Eye to Brain. *Neuron* **37**, 499-511 (2003).
- [7] N.G. Van Kampen, *Stochastic Processes in Physics and Chemistry*, 3rd edition, (North-Holland, 2007)
- [8] S. Coleman, *Aspects of Symmetry*, (Cambridge University Press, 1988)
- [9] A. Dembo, O. Zeitouni, *Large deviation techniques and applications*, 2nd edition, (Springer, 1993)
- [10] L. Paninski. The most likely voltage path and large deviations approximations for integrate-and-fire neurons. *Journal of Computational Neuroscience* **21**, 71-87 (2006).
- [11] L. Paninski, J. Pillow, E. Simoncelli. Maximum likelihood estimation of a stochastic integrate-and-fire neural encoding model. *Neural Computation* **16**, 2533 (2004).
- [12] M. Meister, L. Lagnado, D.A. Baylor. Concerted signaling by retinal ganglion cells. *Science* **270**, 1207-1210 (1995).
- [13] J. Shlens, G.D. Field, J.L. Gauthier, M.I. Grivich, D. Petrusca, A. Sher, A.M. Litke, E.J. Chichilnisky. The structure of multi-neuron firing patterns in primate retina. *Journal of Neuroscience* **26**, 8254-8266 (2006).
- [14] J. Sinova, G. Canright, A.H. MacDonald. Nature of ergodicity breaking in Ising spin glasses as revealed by correlation function spectral properties. *Phys. Rev. Lett.* **85**, 2609 (2000); J. Sinova, G. Canright, H.E. Castillo, A.H. MacDonald. Extensive eigenvalues in spin-spin correlations: A tool for counting pure states in Ising spin glasses. *Phys. Rev. B* **63**, 104427 (2001).
- [15] D.J. Thouless, *Percolation and Localization*, in *Ill-Condensed Matter Proceeding Les Houches*, R. Balian, R. Maynard, G. Toulouse, editors, (North-Holland, 1979).
- [16] K.H. Fisher, J.A. Hertz, *Spin glasses*, (Cambridge University Press, 1991).
- [17] S.K. Ma, *Statistical Mechanics* (World Scientific Publishing Company, 1985)
- [18] D. Sherrington, S. Kirkpatrick. Solvable model of a spin glass. *Phys. Rev. Lett.* **35**, 1792 - 1796 (1975).
- [19] We have to minimize here rather than maximize since the true Lagrange multipliers take imaginary values, the couplings and fields being their imaginary part.
- [20] Equation (4) in the main paper requires the initial conditions for the potentials V_i , e.g. that the potentials are initially equal to their rest value. When the number of recorded spikes for each cell is large, the inferred couplings and currents are largely insensitive to these initial conditions.
- [21] The boundary conditions are now: $V_i(t_{i_0}) = 1$ if $J_{i_0} > 0$, $1 + J_{i_0}$ if $J_{i_0} < 0$, and $V_i(t_{i_1}) = 1$ if $J_{i_1} < 0$, $1 - J_{i_1}$ if $J_{i_1} > 0$.
- [22] The temporal resolution of the recordings (about 1 ms) and the small number of occurrences of pairs of spikes for time-interval bins smaller than 5 ms do not allow us to calculate the coupling when $\Delta t < 5$ ms.
- [23] For instance, in the Curie-Weiss model for the study of the paramagnetic/ferromagnetic transition, all couplings are equal to J/N where J is a constant [17]. In finite-dimensional models couplings are independent of N ; however the average coupling scales as $1/N$ e.g. it is equal to $2dJ/(N-1)$ on a d -dimensional cubic lattice with nearest-neighbour interactions of amplitude J . Couplings may also scale as $1/\sqrt{N}$ when they are random variables with zero mean, as in the Sherrington-Kirkpatrick model for the study of the spin-glass phase [16, 18].
- [24] Notice that there could exist two mirror states with opposite magnetizations even when only one eigenvector is extended. This possibility is ruled out, however, through inspection of the probability that ℓ among N cells fire together in the same bin. A coexistence of opposite states would mean a bimodal distribution for ℓ , with local maxima in $\ell = 0$ and $\ell = N$, which is clearly not seen from the experimental data